The longest-lived Pacific hotspots reveal a plume tail for the largest oceanic plateau

J.G. Konter[a†], V.A. Finlayson[a,b*], K. Konrad[c], M.G. Jackson[d], A.A.P. Koppers[e], P. Wessel[a], M. Bizimis[f], A. Alverson[g], C. Kelley[a]

[a]*Dept. of Earth Sciences, School of Ocean and Earth Science and Technology, University of Hawaii, Manoa, Honolulu, HI 96822, USA*

[b]*Dept. of Geology, University of Maryland, College Park, MD 20742, USA (*Corresponding author; vfinlays@umd.edu)*

[c]*Dept. of Geoscience, University of Nevada Las Vegas, Las Vegas, NV, 89154, USA*

[d]*Dept. of Earth Science, University of California Santa Barbara, Santa Barbara, CA 93106*, *USA*

[e]*College of Earth, Ocean and Atmospheric Sciences, Oregon State University, Corvallis, OR 97331, USA*

[f]*School of the Earth, Ocean, and Environment, University of South Carolina, Columbia, SC, 29208, USA*

[g]*Dept. of Earth, Environmental and Planetary Sciences, Brown University, Providence, RI 02912, USA*

[†]*author deceased*

Volcanic hotspots are thought to initially form by melting in an upwelling mantle plume head followed by melting of the plume tail. Plate motion then generates an age progressive volcanic track originating from a large igneous province that connects to an active hotspot. However, the most voluminous large igneous province, the ~120 Ma Ontong-Java Nui Plateau (OJP-Nui) in the mid-Pacific, appears to lack such a volcanic track. Although the Louisville hotspot track was originally proposed as a candidate, limited constraints for Pacific absolute plate and plume motion prior to 80 Ma suggest a mismatch[1]. Existing Pacific models rely on age-distance data from the continuous Hawaii-Emperor and Louisville volcanic tracks, but their seamounts older than ~80 Ma are now subducted, and elsewhere on the Pacific plate only discontinuous and sparse seamount tracks can be found that formed prior to 80 Ma[2–7]. These existing models require ~1,200 km of latitudinal motion for the Louisville plume to also erupt the OJP-Nui[1], yet paleolatitude estimates from to ~70 Ma to today remain within error of its present location[8,9] and suggest that any major amount of Louisville plume motion should precede that time. Here we provide evidence from geochemistry and eruption ages[9–14] demonstrating that Samoa and Rurutu-Arago are the longest-lived Pacific hotspots that can be traced back to ~120 Ma (and older) in the West Pacific where they subduct into the Mariana Trench. These newly defined tracks provide for an alternative Pacific absolute plate motion model, with better constraints for a plate rotation between 80-100 Ma, and allow us to establish Louisville as the missing volcanic track for OJP-Nui without requiring major plume motion.

Plume-fed hotspots exhibit age-progressive volcanic tracks that often originate from a large igneous province (LIP), which marks a hotspot's inception[15–18]. Eruption of a LIP is thought to correspond to the arrival of the head of a deeply-rooted mantle plume, causing extensive melting in the upper mantle and unusually voluminous eruption comprising the LIP[3,19,20]. The Ontong-Java Plateau (OJP; Fig. 1) once formed greater Ontong-Java Nui (OJP-Nui), together with the Manihiki and Hikurangi plateaus[21]. Despite a proposed plume origin[22,23] there is no obvious age-progressive volcanic track emerging from the plateau. Although the Louisville hotspot was proposed to be related[24], later paleomagnetic and geochemistry data argued against a Louisville hotspot connection with the OJP[25–27]. Recently obtained Louisville paleomagnetic latitudes are constant within error up to ~70 Ma[8], suggesting that any Louisville plume motion should precede 70 Ma. In that timeframe, existing absolute plate motion (APM) models require ~1,200 km of plume motion to place Louisville and OJP in the same original eruptive location[1]. However, more recent geochemical data revealing similar Nd-Pb-Sr systematics between the main phase of the OJP-Nui system and the Louisville Seamount track are permissive of the Louisville-OJP connection[28] (Fig. 2). Additionally, here we show that the two longest-lived Pacific hotspot tracks —Samoa and Rurutu-Arago[9,14] (see below)—yield a new APM model that supports a genetic link between the Louisville hotspot track and OJP-Nui, the largest LIP preserved in the geologic record.

Most existing Pacific APM models rely significantly on the Hawaii-Emperor and Louisville hotspots back to 80 Ma, while unrelated discontinuous volcanic structures are used for Pacific plate motion prior to 80 Ma[2,3,7,18,29,30] (Fig. 1, Extended Data Fig. 1). These structures include the Shatsky Rise, Hess Rise, Mid-Pacific Mountains, Line Islands, Liliuokalani Seamounts, Musician Seamounts, Wake Seamounts, Marshall Islands, and Magellan Seamounts. From these, the Mid-Pacific Mountains and Shatsky Rise erupted near all-ridge triple junctions, while Hess Rise and Musicians Seamounts erupted near-ridge[29–32] (Extended Data Fig. 2). Plume-ridge interactions could significantly displace the upwelling mantle plume[33] such that resulting plume motion is inadvertently included in the APM models. Moreover, the Line Islands lack a clear age progression[34], the Musician Seamounts are complicated by overprinting of deformation-related volcanism[33], and Shatsky Rise was recently suggested to be controlled by seafloor spreading[35]. In summary, all of these structures are unlikely to exclusively represent absolute plate motion, yet the Wake, Marshall, and Magellan seamounts appear to be the only truly intra-plate Pacific hotspots prior to 80 Ma (Extended Data Fig. 2). As we will demonstrate, they represent the Cretaceous portions of two long-lived Pacific hotspots—Samoa and Rurutu-Arago—that can extend Hawaii-Emperor and Louisville anchored Pacific APM models to the 80 to 120 Ma period.

The clearly defined Hawaii-Emperor and Louisville hotspot tracks provide a continuous hotspot record for APM modeling back to approximately 80 Ma, where they subduct into the Kamchatka and Tonga trenches, respectively[8,36] (Fig. 1; Extended Data Fig. 1). However, changing paleomagnetic latitudes[37], predictions of hotspot motion based on Indo-Atlantic hotspots[38], inter-hotspot differences in age progressions and distances[9,39,40], and disparity in the timing of the Hawaii-Emperor bend compared to any known large global plate reorganization[41], all suggest relative motion between these two plumes and the Pacific plate. Supporting this contention, models using global mantle flow to predict plume motions provide a better fit to the actual hotspot tracks across ocean basins than fixed plume models[6]. The improved fit incorporating these geodynamic models suggests that hotspots provide a combined record of plate motion and plume motion[3,5,18].

On the Pacific plate, the Rurutu-Arago volcanic track—defined from young to old by the Cook-Austral Islands, Tuvalu Islands, the Marshall Islands and Wake Seamounts—represents the third long-lasting hotspot in addition to Hawaii-Emperor and Louisville (Fig. 1). Changes in the distance between these hotspots from 60 to 50 Ma suggest that the Hawaii-Emperor hotspot moved more significantly and mostly independently from both Louisville and Rurutu-Arago[9]. However, more critical here is the fact that the Rurutu-Arago and Samoan hotspots can be traced further back into the Cretaceous than Hawaii and Louisville. The older portions of the Rurutu-Arago and Samoa hotspots both extend into the West Pacific, where tracing their tracks through the high density of Cretaceous seamounts has required the mapping out of well-defined age progressions combined with unique geochemical signatures[4,12,14] (Fig. 1, Extended Data Fig. 7, 8).

To this end, we present new isotope geochemistry from seamounts around Wake Island, a critical geological nexus that links the older (>80 Ma) segment of the long-lived Rurutu-Arago hotspot track to the younger (< 80 Ma) portion originating in the Cook-Austral Islands[4,12,14,42,43]. We use this hotspot track, together with the long-lived Samoan hotspot track, to generate a new APM stage pole between 80-100 Ma that resolves the apparent disconnect between OJP-Nui and the Louisville hotspot.

The extreme and distinct hotspot compositions originating in the central Pacific[42] have generated clearly traceable hotspot tracks (Fig. 1, Extended Data Fig. 8). We reveal these tracks by color coding (Fig. 1) based on the $^{87}Sr/^{86}Sr$-$^{143}Nd/^{144}Nd$-$^{206}Pb/^{204}Pb$ isotopic compositions of lavas at each volcano along the hotspot tracks[9–14,44,45]. In particular, high $^{206}Pb/^{204}Pb$ compositions are an identifying feature of the Rurutu-Arago hotspot and can be traced back into the Western Pacific along an age progression (blue, Fig. 1; Extended Data Fig. 8). However, north of the Marshall Islands, a data gap in the Rurutu-Arago hotspot track separated these ≤80 Ma volcanoes from the ≥100 Ma Wake Seamounts, complicating efforts to trace the Rurutu-Arago track prior to 80 Ma. Recent sampling of seamounts around Wake Island fills this gap and new Pb-Sr-Nd isotopic compositions (Methods) of these samples match those of the rest of the Rurutu-Arago hotspot track (Extended Data Fig. 8, Extended Data Fig. 9).

Further west, the Cretaceous Magellan seamounts also span the ~80-100 Ma age range[4] and overlap with the Samoa hotspot in composition. Critically, the age and location of these seamounts matches the predicted track of Samoa (Fig. 1; Extended Data Fig. 8) that can be traced from the present-day location near the northern terminus of the Tonga Trench to ~25 Ma Alexa Bank, west of which the trace of the Samoan hotspot is lost in the Vitiaz Trench. The predicted Samoan hotspot track passes through the OJP, where its large lithospheric thickness[20] likely suppressed Samoan plume melting and volcanic construction[46]. The predicted hotspot therefore is expected to emerge on the north side of the OJP as 80-100 Ma volcanoes, which is consistent with the age and location of the Magellan Seamounts. Further supporting a link to the Samoan hotspot, the Magellan seamounts feature the same unique combination of intermediate $^{206}Pb/^{204}Pb$ and extreme radiogenic $^{87}Sr/^{86}Sr$ isotope compositions observed in Samoan shield lavas[10] (red, Fig. 1), and are capped by late-stage volcanism with a characteristic low $^{206}Pb/^{204}Pb$ and elevated $^{87}Sr/^{86}Sr$ isotope composition[45,47] (green, Fig. 1, Extended Data Fig. 3). Magellan seamount compositions and ages[4] are reassessed here, revealing a Samoan shield to rejuvenated stage isotopic sequence[47] at Hemler and Vlinder Seamounts, while samples obtained from the younger Magellan Seamounts are similar to Samoan late stage rejuvenated compositions (Extended Data Fig. 3).

APM models for the predicted tracks of the high $^{206}Pb/^{204}Pb$ Rurutu-Arago hotspot and the high $^{87}Sr/^{86}Sr$ Samoa hotspot suggest these two hotspot tracks should continue into the Mariana Trench[7,48] (Fig. 1). Geochemical data on Mariana arc volcanoes provides further support that the Rurutu-Arago and Samoa hotspot tracks are subducted near the region proposed by APM models. When the isotopic compositions of the Mariana arc volcanoes are examined, an unusual geographically constrained high $^{206}Pb/^{204}Pb$ anomaly[46,4748,49] and an adjacent high $^{87}Sr/^{86}Sr$ anomaly (which overlaps, but is shifted slightly to the south) are found where the Rurutu-Arago and Samoa hotspot tracks are predicted to subduct based on the revised APM model (Fig. 1, Extended Data Fig. 4). Consistent with the hypothesis that the subduction of seamounts impacts the chemistry of nearby arc volcanoes, the $^{206}Pb/^{204}Pb$ and $^{87}Sr/^{86}Sr$ anomalies in the Mariana arc provide supporting evidence for the presence of the long-lived Rurutu-Arago and Samoan hotspot tracks in the western Pacific during the Early Cretaceous. Furthermore, their offset position in the Mariana arc also supports the presence of a more northerly Rurutu-Arago hotspot track in the western Pacific region predicted by our new APM, which is different from predictions by prior APM models (Fig. 1, Extended Data Fig. 4). Consequently, we now can explore Rurutu-Arago and Samoa as a pair of long-lived parallel (but offset) hotspot tracks, providing a multi-hotspot continuation of APM constraints beyond the 80 Ma limit that is provided by the Hawaii-Emperor and Louisville hotspot tracks.

While the Rurutu-Arago hotspot track is defined by seamounts with related geochemical fingerprints that closely follow APM models back to 80 Ma, existing APM models[7] predict the track to significantly bend to the west around the Wake Seamounts (Extended Data Fig. 4). This region is only sparsely populated by seamounts when compared to the abundance of seamounts around Wake Island and the Wake Seamounts, which provide a clearer morphological continuation of the hotspot track, but more importantly a geochemical match to the Rurutu-Arago hotspot[29,48] (Extended Data Fig. 4). The clear impact of Rurutu-Arago hotspot on Mariana arc compositions[48,49] (Extended Data Fig. 4) suggests that, in contrast to existing APM models, the hotspot followed a more northerly track between 120 and 80 Ma—offset by >1200 km from existing models. This alternative “northern path” (blue path in the Wake Seamounts in Fig. 1, “this study” in Extended Data Fig. 4) for the pre-80 Ma Rurutu-Arago hotspot track provides a unified explanation for all these observations, suggesting that a reconsideration of the APM models is warranted.

The period of plate motion covered by our new data is constrained by the ~80-100 Ma Marshall Island volcanoes and Wake Island area seamounts. Critically, existing ages for the two volcanic chains correspond closely with the 80-100 Ma single plate rotation (stage) of the existing K01 plate motion model[18]. For the period prior to 80 Ma, modern APM models[50] still define motion with the large time-step plate rotations of early models[2,18]. Given the limited availability of ages around Wake Island, we resort to a similar approach as used in the K01 model[3] and calculate plate motion using large time-steps rather than applying a more continuous age models such as WK08[39]. For the 80-100 Ma time interval, we modeled the plate motion by finding the stage pole (5°N, 306°E) that minimizes the difference in Euler pole distance between the actual seamounts and the predicted age progressive paths for the Samoa and Rurutu-Arago hotspot tracks (Methods). Using the new modified APM model, K01m, our results show that the predicted track projects Rurutu-Arago through the Wake area seamounts (blue path in Fig. 1), whereas prior models failed to capture the Wake Islands and seamounts (Extended Data Fig. 4). Due to the southeasterly shift in location of the K01m rotation pole compared to K01, the relative angular distances from the Euler pole to Samoa and Rurutu-Arago have changed in a manner where the resulting predicted path length for Samoa remains similar to older models, while that of Rurutu-Arago lengthens significantly.

The application of this new 80-100 Ma rotation pole to the Louisville hotspot has profound implications for linking the Louisville track to OJP-Nui. While prior plate motion models placed the Louisville hotspot far from OJP at the time of eruption[1], the new 80-100 Ma rotation increases the north-south component of the predicted Louisville path (Fig. 3). As a result, the new K01m model using long-lived intraplate hotspots traces the predicted Louisville hotspot track directly into the center of OJP-Nui by ~120 Ma, the modeled age of formation for the superplateau[21,51]. This is in contrast to existing APM models[3,6,7,50] that all predict a more southerly track (Fig. 3) that falls short of the OJP, most likely because these models incorporate near-ridge large structures (rises) and seamounts in their datasets. An assessment of the fit of individual track segments using backtracking with different APM models confirms this result (Methods; Extended Data Fig. 5). The formation age of OJP-Nui has been estimated based on decades old lower quality ^{40}Ar/^{39}Ar ages and plate reconstructions to be around 120 Ma[21,51], yet recent high-precision geochronology suggests that the main phase of OJP volcanism began around 116 Ma[52]. This makes the reconstructed link between Louisville and OJP-Nui even more likely.

However, in the formation of the Louisville hotspot track from OJP-Nui until present day (Fig. 3), there are two time periods with poor constraints. First, the 80-90 Ma Louisville Seamounts all have subducted into the Tonga Trench, interrupting the direct connection between the OJP and the Louisville seamount track. Second, the location of the earliest portion of the Louisville seamount track between 90-116 Ma depends on whether or not the Manihiki or Hikurangi Plates (and their associated plateaus) rotated during the break-up[1] of OJP-Nui (Fig. 3), and whether there exists an eruptive age progression throughout OJP-Nui given that Manihiki may predate OJP by up to 6 Myr[52]. In either case, the eruptive location of the earliest Louisville track is within the OJP outline and, importantly, we show for the first time that 90-115 Ma seamounts in the Ellice Basin agree with the expected age progression, location, and isotopic signature of Louisville hotspot-related volcanoes in the region[14] (Fig. 2). These seamounts therefore provide the “missing link” connecting the OJP to the start of the Louisville track. The Louisville Seamounts and Ellice Basin seamounts are geochemically similar and plot along the array defined by Manihiki’s Danger Islands and OJP melts (Fig. 2; Methods). Therefore, the Louisville and Ellice Basin seamounts are geochemically and temporally linked to OJP-Nui.

Our demonstrated fit of OJP-Nui to the Louisville hotspot track (Fig. 3; Extended Data Fig. 5) requires no significant plume motion, which agrees with estimates of limited latitudinal motion of this hotspot between ~70-0 Ma[8]. Our new data, and new interpretation of existing data, thus present a simple argument for the genetic connection between Louisville and OJP-Nui. This implies a plume-driven origin for the largest LIP in the geologic record, in contrast to recent arguments for a major role for seafloor spreading in the construction of LIPs, such as Shatsky Rise[35]. Renewed consideration for other Cretaceous "orphan" LIPs—that may still lack obvious volcanic trails—is warranted, in light of the suggested revision to the 80-100 Ma stage pole that may serve to further address identified uncertainties in Pacific APM during the Cretaceous.

ACKNOWLEDGEMENTS

This work was supported by NOAA OER and GFOE, and is part of NSF-OCE project 1912934 to JK and PW. AA was supported by NSF-REU grant 1560196 to PW. MJ was supported by NSF-OCE project 1912931. AK was supported by NSF-OCE 1912932. We thank the crew and the team of ROV pilots and engineers aboard the E/V *Okeanos Explorer*. We thank John VanDecar for handling the editorial process and comments from two anonymous reviewers that improved the manuscript. This manuscript is dedicated to the memory of the first author, Jasper G. Konter.

FIGURES

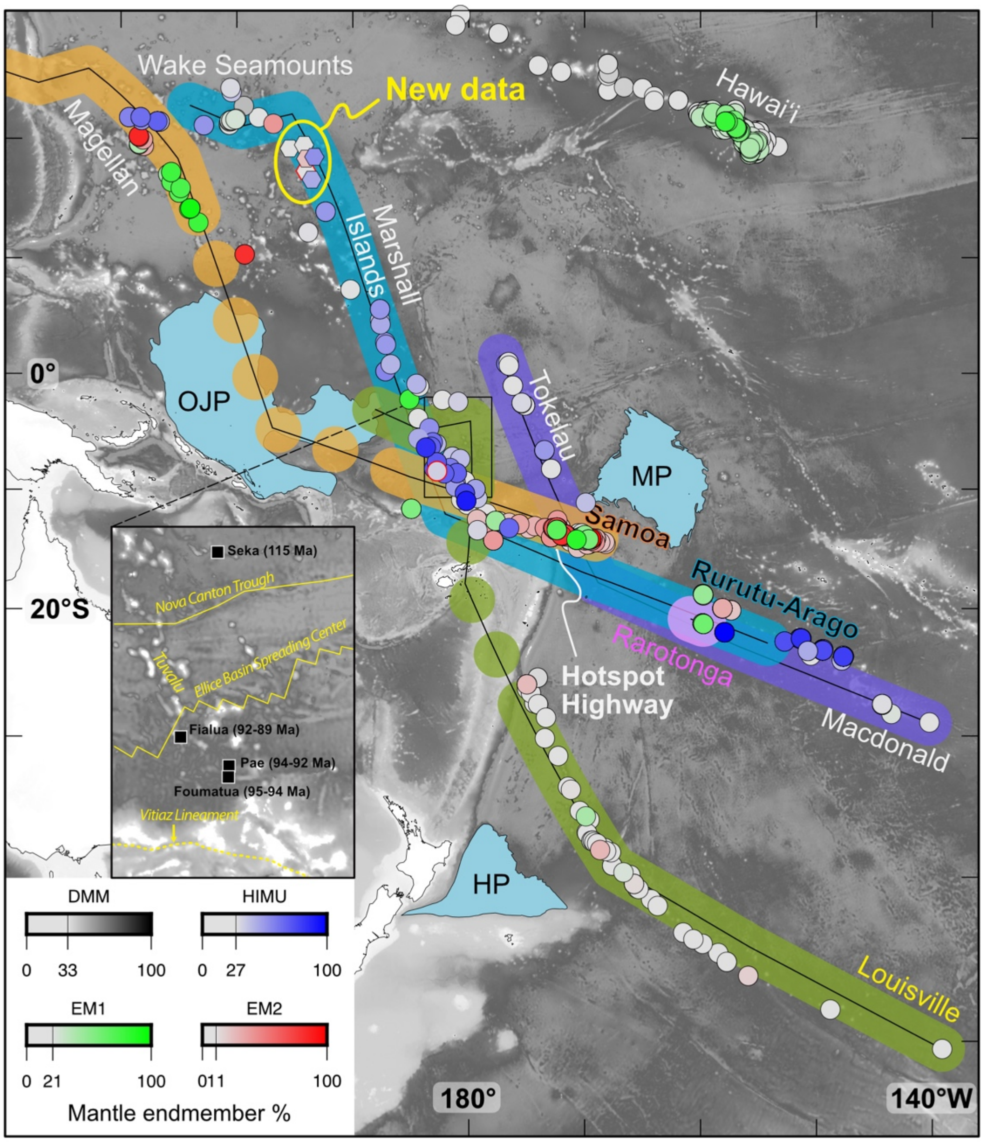

Figure 1*. Pacific hotspot tracks and color-coded geochemical lava flow compositions (bottom right inset, Methods) demonstrate unique signatures for Rurutu-Arago (blue circles) and Samoa (red and green) and thus allow for the effective geochemical tracing of these hotspots, when combined with seamount ages. Ellice Basin Group and the New Wake samples with a red outline are confirmed phosphatized (See Alteration section in Methods) and not considered in discussions of $^{143}Nd/^{144}Nd$ behavior. The known extents of the Rarotonga and Macdonald hotspot tracks are*

provided for reference. The colored tracks show predicted hotspot tracks following the new APM (specifically, 80-100 Ma stage represented by the Wake-Marshall and Magellan areas). The dashed portions of the predicted Louisville hotspot track mark where the track was subducted. For Louisville (green), the updated APM predicts an origin at Ontong-Java Plateau (OJP). The new APM modeling relies on Wake-Marshall and Magellan seamounts, omitting the Shatsky and Mid-Pac groups, and for the first time directly relates the Louisville hotspot to OJP. Hawaiian-Emperor hotspot sample data are shown for reference. See Extended Methods for data sources. ***Inset:*** *Locations and ages of all Ellice Basin Seamounts and Seka Seamount, as confirmed by geochronology, as black squares. The Tuvalu chain, Nova Canton Trough, Ellice Basin Spreading Center, and Vitiaz Lineament are shown in yellow.*

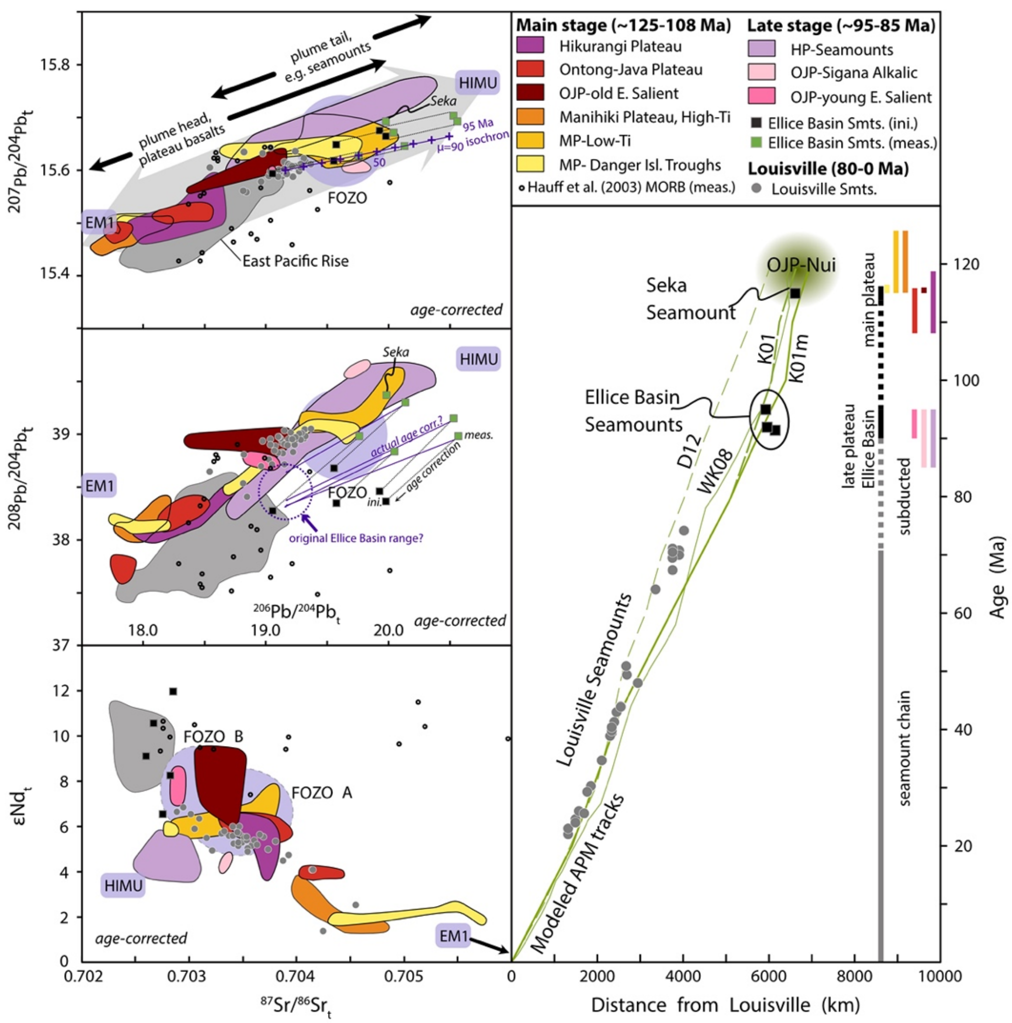

__Figure 2__. Right: Age progression for the Louisville hotspot track (symbols same as in plots). Ellice Basin Seamounts[14] and Seka Seamount[45] are shown. Top: Age-corrected $^{207}Pb/^{204}Pb$ vs. $^{206}Pb/^{204}Pb$ isotope compositions for Ontong Java Nui, and related structures. Middle: Age-corrected $^{208}Pb/^{204}Pb$ vs. $^{206}Pb/^{204}Pb$ isotope compositions for Ontong Java Nui, and related structures. Bottom: $\varepsilon^{143}Nd$ vs. age-corrected $^{87}Sr/^{86}Sr$ for Ontong-Java Nui and related structures. Pb-isotope data for Ontong-Java (OJP), Manihiki (MP), and Hikurangi plateaus (HP), which represent the main pulses of voluminous plateau-building volcanism (~120 and ~90 Ma), are frequently less radiogenic, but extend to radiogenic values in some settings. By contrast, smaller structures such as seamounts are confined to intermediate-to-radiogenic values. Louisville and Ellice Basin seamounts exhibit more radiogenic Pb-isotopes, with Ellice Basin being particularly radiogenic due to seawater U influence, but likely a mixture of FOZO and DMM that originally resembled slightly depleted Louisville-type compositions (see Methods). Green squares are

present-day Ellice Basin compositions, compared to corresponding age-corrected (where possible) compositions. Louisville seamounts overlap directly with some OJP basalts in Pb-Nd-Sr isotope space, and are well within the array of compositions found in the greater combined set of plateaus and structures from OJP, MP and HP. Furthermore, Ellice Basin and Seka seamounts are spatiotemporally linked to the OJP. See Methods for description of isotopic data compared to variations in plume head and plume tail stages of volcanic activity, analysis of Pb-Sr-Nd isotopic systematics in the Ellice Basin Samples, and data sources.

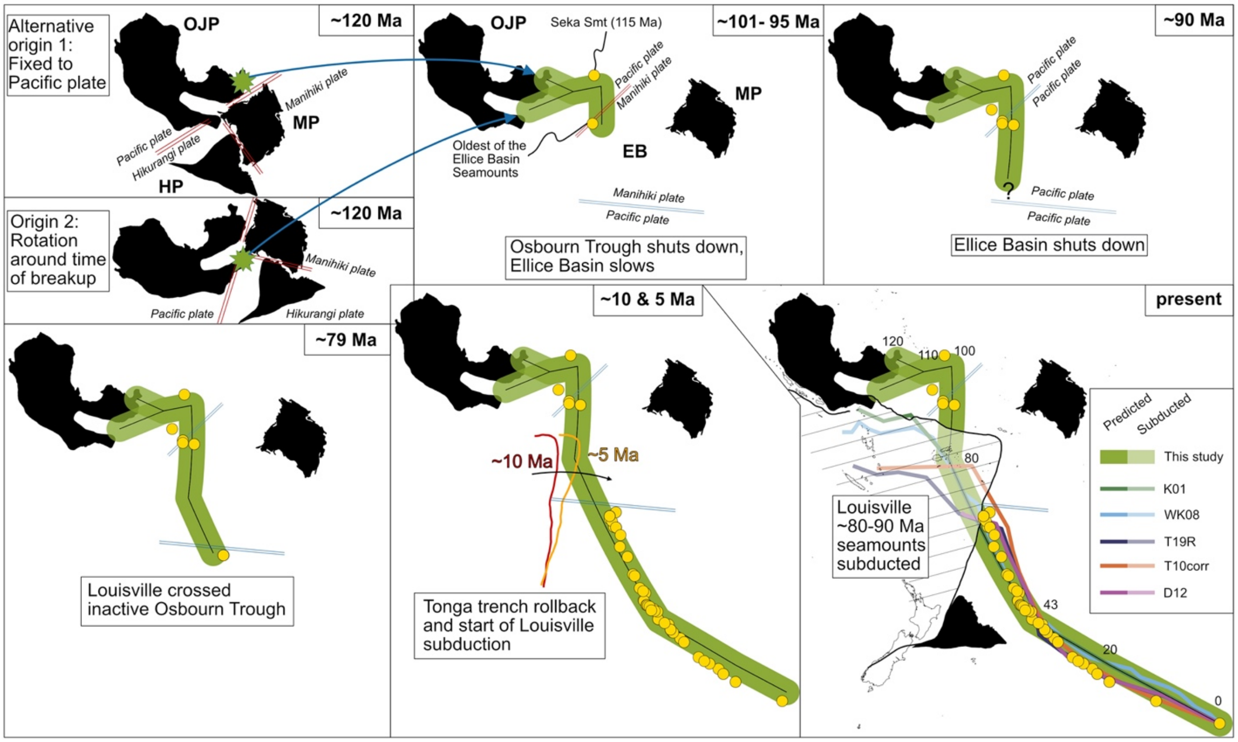

***Figure 3**. Cartoon of Louisville hotspot (green swath) evolution. The revised model predicts that the Louisville hotspot initiated within Ontong Java Plateau (OJP), however the exact initial location is sensitive to whether the plateaus rotated around the time of OJP-Nui breakup[51], so two alternatives are shown for ~120 Ma. By ~95 Ma, the Ellice Basin (EB) had (mostly) opened between OJP and Manihiki Plateau (MP), as suggested by the age of the oldest Ellice Basin Seamounts (95.0 Ma[14])—located centrally in the basin—which we link to the Louisville hotspot. Seka Seamount (115.0 Ma[45]), located at the north end of the basin, is isotopically similar to the Ellice Basin seamounts (suggesting significant Ellice Basin spreading occurred by 115 Ma) and is also linked to the Louisville hotspot. The new model predicts Louisville to be present in the Ellice Basin at this time, progressing to younger ages to the south. The oldest Louisville Seamount erupted at ~79 Ma[8,36], located south of the Osbourn Trough, represents the oldest part of the continuously defined Louisville hotspot track. In the past 5 to 10 Ma, roll-back of the Tonga Trench caused the subduction of any Louisville Seamounts with ages between 79 to 90 Ma, leaving only the older (>90 Ma) Louisville hotspot-related structures in the Ellice Basin and OJP areas preserved. Consequently, the relationship between >79 Ma Louisville hotspot volcanism and the*

paleoridge represented by the Osbourn Trough is unclear. Predicted hotspot tracks show that only the new model tracks Louisville hotspot back to OJP-Nui, specifically the OJP. See Methods for details on this model.

REFERENCES

1. Chandler, M. T., Wessel, P. & Sager, W. W. Analysis of Ontong Java Plateau palaeolatitudes: evidence for large-scale rotation since 123 Ma? *Geophys. J. Int.* **194**, 18–29 (2013).
2. Duncan, R. A. & Clague, D. A. Pacific Plate Motion Recorded by Linear Volcanic Chains. in *The Ocean Basins and Margins: Volume 7A The Pacific Ocean* (eds. Nairn, A. E. M., Stehli, F. G. & Uyeda, S.) 89–121 (Springer US, 1985). doi:10.1007/978-1-4613-2351-8_3.
3. Koppers, A. A. P. *et al.* Mantle plumes and their role in Earth processes. *Nat. Rev. Earth Environ.* **2**, 382–401 (2021).
4. Koppers, A. A. P. & Sager, W. W. Chapter 4.3 - Large-Scale and Long-Term Volcanism on Oceanic Lithosphere. in *Developments in Marine Geology* (eds. Stein, R., Blackman, D. K., Inagaki, F. & Larsen, H.-C.) vol. 7 553–597 (Elsevier, 2014).
5. Tarduno, J., Bunge, H.-P., Sleep, N. & Hansen, U. The Bent Hawaiian-Emperor Hotspot Track: Inheriting the Mantle Wind. *Science* **324**, 50–53 (2009).
6. Doubrovine, P. V., Steinberger, B. & Torsvik, T. H. Absolute plate motions in a reference frame defined by moving hot spots in the Pacific, Atlantic, and Indian oceans. *J. Geophys. Res. Solid Earth* **117**, (2012).
7. Wessel, P. & Kroenke, L. W. Observations of geometry and ages constrain relative motion of Hawaii and Louisville plumes. *Earth Planet. Sci. Lett.* **284**, 467–472 (2009).
8. Koppers, A. A. P., Staudigel, H., Phipps Morgan, J. & Duncan, R. A. Nonlinear 40Ar/39Ar age systematics along the Gilbert Ridge and Tokelau Seamount Trail and the timing of the Hawaii-Emperor Bend. *Geochem. Geophys. Geosystems* **8**, n/a-n/a (2007).

9. Konrad, K. *et al.* On the relative motions of long-lived Pacific mantle plumes. *Nat. Commun.* **9**, 854 (2018).

10. Jackson, M. G. *et al.* Helium and lead isotopes reveal the geochemical geometry of the Samoan plume. *Nature* **514**, 355–358 (2014).

11. Jackson, M. G. *et al.* Samoan hot spot track on a "hot spot highway": Implications for mantle plumes and a deep Samoan mantle source. *Geochem. Geophys. Geosystems* **11**, n/a-n/a (2010).

12. Konter, J. G. & Jackson, M. G. Large volumes of rejuvenated volcanism in Samoa: Evidence supporting a tectonic influence on late-stage volcanism. *Geochem. Geophys. Geosystems* **13**, n/a-n/a (2012).

13. Koppers, A. A. P. *et al.* Limited latitudinal mantle plume motion for the Louisville hotspot. *Nat. Geosci.* **5**, 911–917 (2012).

14. Finlayson, V. A. *et al.* Sr–Pb–Nd–Hf isotopes and 40Ar/39Ar ages reveal a Hawaii–Emperor-style bend in the Rurutu hotspot. *Earth Planet. Sci. Lett.* **500**, 168–179 (2018).

15. Richards, M. A., Duncan, R. A. & Courtillot, V. E. Flood Basalts and Hot-Spot Tracks: Plume Heads and Tails. *Science* **246**, 103–107 (1989).

16. Courtillot, V., Davaille, A., Besse, J. & Stock, J. Three distinct types of hotspots in the Earth's mantle. *Earth Planet. Sci. Lett.* **205**, 295–308 (2003).

17. Konter, J. G. & Becker, T. W. Shallow lithospheric contribution to mantle plumes revealed by integrating seismic and geochemical data. *Geochem. Geophys. Geosystems* **13**, n/a-n/a (2012).

18. Koppers, A. A. P., Morgan, J. P., Morgan, J. W. & Staudigel, H. Testing the fixed hotspot hypothesis using 40Ar/39Ar age progressions along seamount trails. *Earth Planet. Sci. Lett.* 16 (2001).
19. Campbell, I. H., Griffiths, R. W. & Hill, R. I. Melting in an Archaean mantle plume: heads it's basalts, tails it's komatiites. *Nature* **339**, 697–699 (1989).
20. Coffin, Millard F. & Eldholm, Olav. Large igneous provinces: Crustal structure, dimensions, and external consequences. *Rev. Geophys.* **32**, 1–36 (1994).
21. Taylor, B. The single largest oceanic plateau: Ontong Java–Manihiki–Hikurangi. *Earth Planet. Sci. Lett.* **241**, 372–380 (2006).
22. Mahoney, J. J. & Spencer, K. J. Isotopic evidence for the origin of the Manihiki and Ontong Java oceanic plateaus. *Earth Planet. Sci. Lett.* **104**, 196–210 (1991).
23. Golowin, R. *et al.* Geochemistry of deep Manihiki Plateau crust: Implications for compositional diversity of large igneous provinces in the Western Pacific and their genetic link. *Chem. Geol.* **493**, 553–566 (2018).
24. Henderson, L. & Gordon, R. G. Oceanic plateaus and the motion of the Pacific plate with respect to the hotspots. *Eos Trans. Am. Geophys. Union* **62**, 1028 (1981).
25. Antretter, M., Riisager, P., Hall, S., Zhao, X. & Steinberger, B. Modelled palaeolatitudes for the Louisville hot spot and the Ontong Java Plateau. *Geol. Soc. Lond. Spec. Publ.* **229**, 21–30 (2004).
26. Kroenke, L. W., Wessel, P. & Sterling, A. Motion of the Ontong Java Plateau in the hot-spot frame of reference: 122 Ma-present. *Geol. Soc. Lond. Spec. Publ.* **229**, 9–20 (2004).

27. Neal, C., Mahoney, J., Kroenke, L., Duncan, R. & Petterson, M. The Ontong Java Plateau. *Wash. DC Am. Geophys. Union Geophys. Monogr. Ser.* 183–216 (1997) doi:10.1029/GM100p0183.
28. Vanderkluysen, L. *et al.* Louisville Seamount Chain: Petrogenetic processes and geochemical evolution of the mantle source. *Geochem. Geophys. Geosystems* **15**, 2380–2400 (2014).
29. Koppers, A. A. P., Staudigel, H., Pringle, M. S. & Wijbrans, J. R. Short-lived and discontinuous intraplate volcanism in the South Pacific: Hot spots or extensional volcanism? *Geochem. Geophys. Geosystems* **4**, n/a-n/a (2003).
30. Sager, W. W. *et al.* Oceanic plateau formation by seafloor spreading implied by Tamu Massif magnetic anomalies. *Nat. Geosci.* **12**, 661–666 (2019).
31. Kopp, H. *et al.* Fossil hot spot-ridge interaction in the Musicians Seamount Province: Geophysical investigations of hot spot volcanism at volcanic elongated ridges. *J. Geophys. Res. Solid Earth* **108**, (2003).
32. O'Connor, J. M. *et al.* Deformation-related volcanism in the Pacific Ocean linked to the Hawaiian–Emperor bend. *Nat. Geosci.* **8**, 393–397 (2015).
33. Fletcher, M., Wyman, D. A. & Zahirovic, S. Mantle plumes, triple junctions and transforms: A reinterpretation of Pacific Cretaceous – Tertiary LIPs and the Laramide connection. *Geosci. Front.* **11**, 1133–1144 (2020).
34. Davis, A. S., Gray, L. B., Clague, D. A. & Hein, J. R. The Line Islands revisited: New 40Ar/39Ar geochronologic evidence for episodes of volcanism due to lithospheric extension. *Geochem. Geophys. Geosystems* **3**, 1–28 (2002).
35. Sager, W. W. What built Shatsky Rise, a mantle plume or ridge tectonics? 15.

36. Heaton, D. E. & Koppers, A. a. P. High-Resolution 40Ar/39Ar Geochronology of the Louisville Seamounts IODP Expedition 330 Drill Sites: Implications for the Duration of Hot Spot-related Volcanism and Age Progressions. *Geochem. Geophys. Geosystems* **20**, 4073–4102 (2019).

37. Bono, R. K., Tarduno, J. A. & Bunge, H.-P. Hotspot motion caused the Hawaiian-Emperor Bend and LLSVPs are not fixed. *Nat. Commun.* **10**, 3370 (2019).

38. Cande, S. C., Raymond, C. A., Stock, J. & Haxby, W. F. Geophysics of the Pitman Fracture Zone and Pacific-Antarctic Plate Motions During the Cenozoic. *Sci. New Ser.* **270**, 947–953 (1995).

39. Wessel, P. & Kroenke, L. W. Pacific absolute plate motion since 145 Ma: An assessment of the fixed hot spot hypothesis. *J. Geophys. Res.* **113**, (2008).

40. O'Connor, J. M. *et al.* Constraints on past plate and mantle motion from new ages for the Hawaiian-Emperor Seamount Chain: HAWAIIAN-EMPEROR SEAMOUNT CHAIN AGES. *Geochem. Geophys. Geosystems* **14**, 4564–4584 (2013).

41. Müller, D. *et al.* Ocean Basin Evolution and Global-Scale Plate Reorganization Events Since Pangea Breakup. *Annu. Rev. Earth Planet. Sci.* **44**, 107–138 (2016).

42. Staudigel, H., Koppers, A. A. P., Plank, T. A. & Hanan, B. B. Seamounts in the Subduction Factory. *Oceanography* **23**, 176–181 (2010).

43. Janney, P. E. & Castillo, P. R. Isotope geochemistry of the Darwin Rise seamounts and the nature of long-term mantle dynamics beneath the south central Pacific. *J. Geophys. Res. Solid Earth* **104**, 10571–10589 (1999).

44. Jackson, M. G. *et al.* The return of subducted continental crust in Samoan lavas. *Nature* **448**, 684–687 (2007).

45. Konter, J. G. *et al.* One hundred million years of mantle geochemical history suggest the retiring of mantle plumes is premature. *Earth Planet. Sci. Lett.* **275**, 285–295 (2008).

46. Price, A. A. *et al.* Distinguishing Volcanic Contributions to the Overlapping Samoan and Cook-Austral Hotspot Tracks. *J. Petrol.* **63**, egac032 (2022).

47. Reinhard, A. A. *et al.* “Petit Spot” Rejuvenated Volcanism Superimposed on Plume-Derived Samoan Shield Volcanoes: Evidence From a 645-m Drill Core From Tutuila Island, American Samoa. *Geochem. Geophys. Geosystems* **20**, 1485–1507 (2019).

48. Staudigel, H. *et al.* The longevity of the South Pacific isotopic and thermal anomaly. *Earth Planet. Sci. Lett.* **102**, 24–44 (1991).

49. Stern, R. J., Fouch, M. J. & Klemperer, S. L. An overview of the Izu-Bonin-Mariana subduction factory. *Wash. DC Am. Geophys. Union Geophys. Monogr. Ser.* **138**, 175–222 (2003).

50. Torsvik, T. H. *et al.* Pacific-Panthalassic Reconstructions: Overview, Errata and the Way Forward. *Geochem. Geophys. Geosystems* **20**, 3659–3689 (2019).

51. Chandler, M. T. *et al.* Reconstructing Ontong Java Nui: Implications for Pacific absolute plate motion, hotspot drift and true polar wander. *Earth Planet. Sci. Lett.* **331–332**, 140–151 (2012).

52. Davidson, P. C., Koppers, A. A. P., Sano, T. & Hanyu, T. A younger and protracted emplacement of the Ontong Java Plateau. *Science* **380**, 1185–1188 (2023).

53. Konter, J. G. & Storm, L. P. High precision 87Sr/86Sr measurements by MC-ICP-MS, simultaneously solving for Kr interferences and mass-based fractionation. *Chem. Geol.* **385**, 26–34 (2014).

54. Béguelin, P., Bizimis, M., Beier, C. & Turner, S. Rift–plume interaction reveals multiple generations of recycled oceanic crust in Azores lavas. *Geochim. Cosmochim. Acta* **218**, 132–152 (2017).

55. Allègre, C. J., Hamelin, B., Provost, A. & Dupré, B. Topology in isotopic multispace and origin of mantle chemical heterogeneities. *Earth Planet. Sci. Lett.* **81**, 319–337 (1987).

56. Hart, S. R. *et al.* Genesis of the Western Samoa seamount province: age, geochemical fingerprint and tectonics. *Earth Planet. Sci. Lett.* **227**, 37–56 (2004).

57. Zindler, A. & Hart, Stan. Chemical Geodynamics. 79 (1986).

58. Hanan, B. B. & Graham, D. W. Lead and Helium Isotope Evidence from Oceanic Basalts for a Common Deep Source of Mantle Plumes. *Sci. New Ser.* **272**, 991–995 (1996).

59. Smith, W. H. F., Staudigel, H., Watts, A. B. & Pringle, M. S. The Magellan seamounts: Early Cretaceous record of the South Pacific isotopic and thermal anomaly. *J. Geophys. Res. Solid Earth* **94**, 10501–10523 (1989).

60. Morgan, W. Jason. Deep Mantle Convection Plumes and Plate Motions. *AAPG Bull.* **56**, (1972).

61. Steinberger, B., Sutherland, R. & O'Connell, R. J. Prediction of Emperor-Hawaii seamount locations from a revised model of global plate motion and mantle flow. *Nature* **430**, 167–173 (2004).

62. Duncan, R. A. & Keller, R. A. Radiometric ages for basement rocks from the Emperor Seamounts, ODP Leg 197. *Geochem. Geophys. Geosystems* **5**, (2004).

63. Seton, M. *et al.* Global continental and ocean basin reconstructions since 200Ma. *Earth-Sci. Rev.* **113**, 212–270 (2012).

64. Hochmuth, K., Gohl, K. & Uenzelmann-Neben, G. Playing jigsaw with Large Igneous Provinces-A plate tectonic reconstruction of Ontong Java Nui, West Pacific. *Geochem. Geophys. Geosystems* **16**, 3789–3807 (2015).

65. Zhang, G.-L. & Li, C. Interactions of the Greater Ontong Java mantle plume component with the Osbourn Trough. *Sci. Rep.* **6**, 37561 (2016).

66. Wobbe, F., Gohl, K., Chambord, A. & Sutherland, R. Structure and breakup history of the rifted margin of West Antarctica in relation to Cretaceous separation from Zealandia and Bellingshausen plate motion. *Geochem. Geophys. Geosystems* **13**, (2012).

67. Mortimer, N. *et al.* Late Cretaceous oceanic plate reorganization and the breakup of Zealandia and Gondwana. *Gondwana Res.* **65**, 31–42 (2019).

68. Benyshek, E. K., Wessel, P. & Taylor, B. Tectonic Reconstruction of the Ellice Basin. *Tectonics* **38**, 3854–3865 (2019).

69. Konter, J. G. *et al.* Geochemical stages at Jasper Seamount and the origin of intraplate volcanoes. *Geochem. Geophys. Geosystems* **10**, n/a-n/a (2009).

70. Koppers, A. A. P. Asynchronous Bends in Pacific Seamount Trails: A Case for Extensional Volcanism? *Science* **307**, 904–907 (2005).

71. Hart, S. R., Hauri, E. H., Oschmann, L. A. & Whitehead, J. A. Mantle Plumes and Entrainment: Isotopic Evidence. *Science* **256**, 517–520 (1992).

72. Koppers, A. A. P. *et al.* Samoa reinstated as a primary hotspot trail. *Geology* **36**, 435 (2008).

73. Koppers, A. A. P., Staudigel, H., Wijbrans, J. R. & Pringle, M. S. The Magellan seamount trail: implications for Cretaceous hotspot volcanism and absolute Pacific plate motion. *Earth Planet. Sci. Lett.* **163**, 53–68 (1998).

74. Koppers, A. A. P. *et al.* New ^{40}Ar/^{39}Ar age progression for the Louisville hot spot trail and implications for inter-hot spot motion. *Geochem. Geophys. Geosystems* **12**, n/a-n/a (2011).

75. Koppers, A. A. P. *et al.* Age systematics of two young en echelon Samoan volcanic trails. *Geochem. Geophys. Geosystems* **12**, n/a-n/a (2011).

76. Coffin, M. F. *et al.* Large igneous provinces and scientific ocean drilling: status quo and a look ahead. *Oceanography* **19**, 150–160 (2006).

77. Harrison, L. N., Weis, D. & Garcia, M. O. The link between Hawaiian mantle plume composition, magmatic flux, and deep mantle geodynamics. *Earth Planet. Sci. Lett.* **463**, 298–309 (2017).

78. Harrison, L. N. & Weis, D. The Size and Emergence of Geochemical Heterogeneities in the Hawaiian Mantle Plume Constrained by Sr-Nd-Hf Isotopic Variation Over ~47 Million Years. *Geochem. Geophys. Geosystems* **19**, 2823–2842 (2018).

79. Harrison, L. N., Weis, D. & Garcia, M. O. The multiple depleted mantle components in the Hawaiian-Emperor chain. *Chem. Geol.* **532**, 119324 (2020).

80. Wei, X. *et al.* Co-Occurrence of HIMU and EM1 Components in a Single Magellan Seamount: Implications for the Formation of West Pacific Seamount Province. *J. Petrol.* **63**, egac022 (2022).

81. Hémond, C., Devey, C. W. & Chauvel, C. Source compositions and melting processes in the Society and Austral plumes (South Pacific Ocean): Element and isotope (Sr, Nd, Pb, Th) geochemistry. *Chem. Geol.* **115**, 7–45 (1994).

82. Bonneville, A., Dosso, L. & Hildenbrand, A. Temporal evolution and geochemical variability of the South Pacific superplume activity. *Earth Planet. Sci. Lett.* **244**, 251–269 (2006).

83. Buff, L. *et al.* "Missing links" for the long-lived Macdonald and Arago hotspots, South Pacific Ocean. *Geology* **49**, 541–544 (2021).

84. Class, C. & Lehnert, K. PetDB expert MORB (mid-ocean ridge basalt) compilation. (2012).

85. Mahoney, J. J., Storey, M., Duncan, R. A., Spencer, K. J. & Pringle, M. Geochemistry and age of the Ontong Java Plateau. *Wash. DC Am. Geophys. Union Geophys. Monogr. Ser.* **77**, 233–261 (1993).

86. Tejada, M. L. G., Mahoney, J. J., Duncan, R. A. & Hawkins, M. P. Age and Geochemistry of Basement and Alkalic Rocks of Malaita and Santa Isabel, Solomon Islands, Southern Margin of Ontong Java Plateau. *J. Petrol.* **37**, 361–394 (1996).

87. Tejada, M. L. G. *et al.* Pin-pricking the elephant: evidence on the origin of the Ontong Java Plateau from Pb-Sr-Hf-Nd isotopic characteristics of ODP Leg 192 basalts. *Geol. Soc. Lond. Spec. Publ.* **229**, 133–150 (2004).

88. Tejada, M. L. G. Basement Geochemistry and Geochronology of Central Malaita, Solomon Islands, with Implications for the Origin and Evolution of the Ontong Java Plateau. *J. Petrol.* **43**, 449–484 (2002).

89. Hoernle, K. *et al.* Age and geochemistry of volcanic rocks from the Hikurangi and Manihiki oceanic Plateaus. *Geochim. Cosmochim. Acta* **74**, 7196–7219 (2010).

90. Timm, C. *et al.* Age and geochemistry of the oceanic Manihiki Plateau, SW Pacific: New evidence for a plume origin. *Earth Planet. Sci. Lett.* **304**, 135–146 (2011).

91. Ingle, S. *et al.* Depleted mantle wedge and sediment fingerprint in unusual basalts from the Manihiki Plateau, central Pacific Ocean. *Geology* **35**, 595 (2007).

92. Hauff, F., Hoernle, K. & Schmidt, A. Sr-Nd-Pb composition of Mesozoic Pacific oceanic crust (Site 1149 and 801, ODP Leg 185): Implications for alteration of ocean crust and the

input into the Izu-Bonin-Mariana subduction system. *Geochem. Geophys. Geosystems* **4**, (2003).

93. Beier, C., Vanderkluysen, L., Regelous, M., Mahoney, J. J. & Garbe-Schönberg, D. Lithospheric control on geochemical composition along the Louisville Seamount Chain. *Geochem. Geophys. Geosystems* **12**, n/a-n/a (2011).
94. Kingsley, R. H., Blichert-Toft, J., Fontignie, D. & Schilling, J.-G. Hafnium, neodymium, and strontium isotope and parent-daughter element systematics in basalts from the plume-ridge interaction system of the Salas y Gomez Seamount Chain and Easter Microplate. *Geochem. Geophys. Geosystems* **8**, n/a-n/a (2007).
95. Regelous, M. Geochemistry of Lavas from the Emperor Seamounts, and the Geochemical Evolution of Hawaiian Magmatism from 85 to 42 Ma. *J. Petrol.* **44**, 113–140 (2003).
96. Nebel, O. *et al.* Coupled Hf–Nd–Pb isotope co-variations of HIMU oceanic island basalts from Mangaia, Cook-Austral islands, suggest an Archean source component in the mantle transition zone. *Geochim. Cosmochim. Acta* **112**, 87–101 (2013).
97. Sun, S. -s. & McDonough, W. F. Chemical and isotopic systematics of oceanic basalts: implications for mantle composition and processes. *Geol. Soc. Lond. Spec. Publ.* **42**, 313–345 (1989).
98. Hart, S. R. & Blusztajn, J. Age and geochemistry of the mafic sills, ODP site 1276, Newfoundland margin. *Chem. Geol.* **235**, 222–237 (2006).
99. Ruellan, E., Delteil, J., Wright, I. & Matsumoto, T. From rifting to active spreading in the Lau Basin – Havre Trough backarc system (SW Pacific): Locking/unlocking induced by seamount chain subduction. *Geochem. Geophys. Geosystems* **4**, (2003).

100. Torsvik, T. H., Steinberger, B., Gurnis, M. & Gaina, C. Plate tectonics and net lithosphere rotation over the past 150My. *Earth Planet. Sci. Lett.* **291**, 106–112 (2010).

101. Müller, R. D. *et al.* A Global Plate Model Including Lithospheric Deformation Along Major Rifts and Orogens Since the Triassic. *Tectonics* **38**, 1884–1907 (2019).

102. Regelous, M. *et al.* Mantle dynamics and mantle melting beneath Niuafo'ou Island and the northern Lau back-arc basin. *Contrib. Mineral. Petrol.* **156**, 103–118 (2008).

103. Tarduno, J. A. *et al.* The Emperor Seamounts: Southward Motion of the Hawaiian Hotspot Plume in Earth's Mantle. *Sci. New Ser.* **301**, 1064–1069 (2003).

104. Jochum, K. P. *et al.* GeoReM: A New Geochemical Database for Reference Materials and Isotopic Standards. *Geostand. Geoanalytical Res.* **29**, 333–338 (2005).

105. Todt, W., Cliff, R., Hanser, A. & Hofmann, A. Evaluation of a 202Pb - 205Pb double spike for high - Precision lead isotope analysis. *Geophys. Monogr. Ser.* **95**, 429–437 (1996).

106. Münker, C., Weyer, S., Scherer, E. & Mezger, K. Separation of high field strength elements (Nb, Ta, Zr, Hf) and Lu from rock samples for MC-ICPMS measurements. *Geochem. Geophys. Geosystems* **2**, (2001).

107. Blichert-Toft, J. & Albarède, F. The Lu-Hf isotope geochemistry of chondrites and the evolution of the mantle-crust system. *Earth Planet. Sci. Lett.* **148**, 243–258 (1997).

METHODS

Sample analysis

Samples were collected with an ROV, aboard the NOAA exploration vessel *Okeanos Explorer*, during expedition EX1606 to the Wake Island Unit of the U.S. Pacific Remote Island Marine National Monument. Dive samples were cut open and the six least altered samples were selected. Pb-Sr-Nd isotopic compositions were obtained following mechanical and chemical procedures to remove seafloor alteration contributions[4] and previously detailed elemental separation procedures[53]. In short, small piece from the center of each sample was crushed, altered pieces were removed by hand-picking, the clean fraction was acid-leached, and subsequently dissolved for Pb separation using Eichrom resin. Isotope measurements were performed on a Nu Plasma HR MC-ICP-MS at University of Hawaiʻi at Mānoa (Pb) and a ThermoFinnegan NeptunePlus at University of South Carolina (Sr, Nd, and Hf[54]). Additional analytical details, results and brief sample characterizations, including assumed age-corrected isotopic ratios for the EX1606 samples, are reported in the Extended Data Table 1. Isotopic behavior shown in Extended Data Fig. 8 and Extended Data Fig. 9 demonstrate the compositional agreement between the new samples characterized here, and published data for the Rurutu-Arago hotspot track.

Trace elements were collected using a ThermoFinnegan Element2 at University of South Carolina on aliquots of powders lightly leached with 0.1N HCl in a sonic bath for 20 minutes to mitigate any low-temperature overprinting by seawater without compromising the primary bulk composition.

Color coding

In order to show the compositional distinction between the hotspot tracks in the western Pacific, as well as to show how compositions backtrack around present-day hotspots, the radiogenic isotope composition of the tracks are color-coded[14,17,45]. The technique focuses on use of $^{87}Sr/^{86}Sr$-$^{143}Nd/^{144}Nd$-$^{206}Pb/^{204}Pb$ isotope compositions, because principal component analysis shows these represent the largest compositional variations in hotspots[55,56]. In this space, hotspots scatter between four extreme end-member compositions: HIMU, EMI, EMII, and DMM[57]. Each hotspot's samples define an elongated, prolate ellipsoid, and these ellipsoids (32 in the global hotspot database) radiate from a central region, known as FOZO[56] or C[58]. The color-coding[45] assigns a level of color-saturation based on its distance from this center, while the color depends on the end-member that a particular sample trends closest to (Fig. 1 inset). Compositions that are on the trend toward an end-member, but cannot be resolved from the central FOZO[56] or C[58] component are colored grey (note that the cutoff percentages for each end-member are shown on colorbars in the Fig. 1 inset). Using this color coding approach results in a "blue" color for symbols, representing HIMU compositions, which dominate hotspot track that run from the Cook-Austral Islands in the central equatorial Pacific to seamount tracks in the Western Pacific. This HIMU compositional "signature band" in map view (i.e., as the blue symbols the represent the Rurutu-Arago HIMU hotspot track form a "band" across the south Pacific and into the Western Pacific Seamount Province) is consistent with predicted absolute plate motion (APM) in the Pacific until at least 80 Ma, and forms the basis for our investigation that links the Wake area seamounts in the Western Pacific to the long-lived Rurutu/Arago hotspot that also includes the Tuvalu islands and the Gilbert Ridge seamount track. In addition, the red (representingEM2) and green (EM1) compositional color coding for Samoa appears in young Samoan hotspot lavas and also appears in the far western Pacific in the Cretaceous Magellan seamounts. Recent work in Samoa has shown a temporal compositional evolution from red (EM2) to green (EM1), representing the evolution from shield to rejuvenated stage of volcanism at Samoa, and the same is observed in the Western Pacific when compositions and ages are assessed (Hemler and Vlinder seamounts[4,59]; Extended Data Fig. 5).

Absolute Plate Motion Modeling

Although initial models[2,60] already showed that simple plate rotations do fit the shapes of several hotspot tracks, recent models[39] have evolved to include more sophisticated techniques to find the best-fit absolute plate motion models by using multiple hotspots and by resolving continuous plate rotations from both seamount locations and ages. In addition, some models include large scale mantle flow, comparisons between ocean basins, and plume motion[6,38,61]. For the Pacific plate >80 Ma, little data are available as neither Hawaii nor Louisville continue past 80 Ma[88,62], and plate circuits that would allow comparison with the Indo-Atlantic hotspot do not extend beyond this time either[6]. In most existing models, the time period prior to 80 Ma is populated with data from Shatsky Rise and the Mid-Pacific Mountains, yet their respective structures were within ~1,000 km of the ridge system[63] (Extended Data Fig. 1) and during their formation these tracks are likely to have been influenced by ridge interaction[55]. However, the Rurutu-Arago and Samoa hotspots do define tracks in this age range that are clearly distinct in their isotopic compositions (Fig. 1; see Section on Color Coding) and that are truly intraplate prior to 80 Ma (Extended Data Fig. 1). We conclude that Rurutu-Arago and Samoa therefore are a more faithful reflection of APM for the Pacific plate.

The presence of two hotspot tracks—Samoa and Rurutu-Arago—provides a means to fit a plate rotation for 80-100 Ma that fits both hotspots, thereby relying on their common motion to define an APM pole for that period. Unlike younger volcanic tracks, Samoa and Rurutu-Arago provide enough data to outline the overall hotspot track; however, the sample and data density are low, such that constraints are lacking for a high-resolution model[39]. Instead, the available data here are used to identify an 80-100 Ma section in both volcanic tracks (Extended Data Fig. 6; Extended Data Tables 2, 3), after which a least-squares method is used to find the best-fit rotation pole for both hotspots. The method[18] consists of finding the best-fit pole that minimizes the variance in calculated angular (seamount-pole) distances, in the least-squares sense. The solution is found with a grid-search algorithm that tests

$$var(d_{ij}) = \sum_{j=1}^{M} \sum_{i=1}^{N} \frac{\left(d_i^j - d_{mean}^j\right)^2}{N}$$

which calculates the variance in distance (d) for all seamounts in the 80-100 Ma track segment relative to the mean distance for a given hotspot (d_{mean}). The variation in distance per hotspot is normalized by the number of seamounts (N) per hotspot. This technique suggests a best-fit stage pole west of the Samoa-related seamounts, near the equator (5.0°N, 54.0°W, rotation rate: 0.85°/Myr; Extended Data Table 2). The resulting K01m APM model is a much better fit to the two hotspot tracks, particularly for the Rurutu-Arago hotspot, where the predicted track now bends to the west at ~100 Ma, just northwest of Wake Island (Fig. 1, Extended Data Fig. 4, 5). Due to the shift in the rotation pole compared to prior models, the angular distance from the pole to the Rurutu-Arago track and the new rotation rate provide a better fit to the seamount track. Despite these improvements, several issues must be considered before the new model can be applied to the Louisville hotspot track.

Plate motion southeast of OJP involved more than just the Pacific plate. During the break-up of OJP-Nui, the Manihiki and Hikurangi plates formed, while the Chazca plate resided immediately to the east[50]. It is important to evaluate whether these plates moved independently with respect to the Pacific plate while the Ellice Basin was located over the Louisville hotspot. The relevant plates/microplates are associated with the break-up of OJP-Nui. The oldest Louisville Seamounts (ranging in age from 1 to 79 Ma[8,36]) are located south of the Osbourn Trough and west of the Wishbone Scarp, representing a small plate forming as Hikurangi separated from OJP. However, true spreading on the Osbourn Trough may have ceased between 101-100 Ma[64,65]. Any further rotation of this plate ceased between ~84 Ma-79 Ma[66,67], so Louisville Seamounts younger than 79 Ma formed after this plate was already part of the Pacific plate. Thus, Louisville Seamounts after 79 Ma properly represent Pacific plate motion with respect to the Louisville hotspot. The only other area where older volcanoes related to Louisville may be exposed is in the area of the Ellice Basin between OJP and Manihiki[14]. However, the exact timing of cessation of motion between the separating plateaus is not well constrained[21]. The sparse age information from the Ellice Basin includes the 95 Ma Foumatua seamount located on the fossil ridge system[14], constraining a minimum age of ~95 Ma for when seafloor spreading in the Ellice Basin shut down, as suggested by models based on seafloor fabric[68]. Critically, Foumatua Seamount is part of a group of similarly aged "Ellice Basin Seamounts" that have an isotopic composition that overlaps with that of the younger Louisville Seamounts[14] (Fig. 2).These seamounts are located where our APM model predicts the Louisville hotspot around ~95 Ma, and the seamounts are also age-progressive with the Louisville seamounts (Fig. 1, 2). The 115 Ma Seka Seamount, located north of the Ellice Basin fossil ridge and near the southern terminus of Gilbert Ridge several hundred kilometers east of the OJP, places the underlying seafloor – and westward motion of the OJP fragment relative to the plume – at a minimum age of 115 Ma, thus indicating that early stage Ellice Basin opening was rapid.

Due to the known wide variation in paleomagnetic latitude estimates for OJP[51], any microplate considerations prior to ~100 Ma are underconstrained at best. Either the plateaus rotated around the time of break-up[51], or OJP was already fixed with respect to the Pacific plate[67]. Regardless, the sheer size of the entire Ontong Java Nui combined structure is so large that neither a rotation of the plateaus, nor ongoing spreading in the Ellice Basin until ~100 Ma, would place the predicted Louisville hotspot outside of the outline of the combined OJP-Nui plateau (or even

OJP by itself) at 120 Ma (Fig. 3). This is mainly due to the final east-west length of the 100-120 Ma predicted Louisville hotspot track being shorter than the width of OJP, which is thought to have largely moved east-west[21,68] (Fig. 1). In Fig. 3, the approximate eruptive locations are also shown assuming OJP either was fixed from ~120 Ma, or only rotated around a pole internal to the plateau[51]. Intriguingly, the rotation of the plateaus places the eruptive location at ~120 Ma near the triple junction between the three plateaus.

Backtracking

Individual volcanoes that have been age-dated can be backtracked to their original eruptive location, by rotating present-day volcano locations in the opposite direction of plate motion according to the sequence of APM model rotations. Existing APM models are used as stage pole rotations to accommodate volcanic ages in between supplied finite rotations. Instead of each volcano backtracking to the same single hotspot location, this process generates clusters due to various geologic and measurement uncertainties, such as: (1) volcanic age precision and accuracy, (2) extended eruption of single volcanoes (up to 7 Ma[69]), (3) offset between sampled rift zone eruptions and the central crater, and (4) lithospheric structure offsetting volcano from mantle source[4,70]. Cumulatively, these uncertainties could cause hundreds of km of scatter in backtracked locations that cluster around the present-day hotspot[45].

Two categories of structures were backtracked here: (1) individual volcanoes of Rurutu-Arago, Samoa and Louisville, and (2) the OJP as a single structure. For the individual hotspot volcanoes (Extended Data Table 3), published $^{40}Ar/^{39}Ar$ ages were used[9,71–75], while symbols for reconstructed volcanoes are colored (see Color Coding) based on their isotopic composition[10–12,14,44]. This highlights the compositional groups by color, matching present-day hotspot locations at Samoa and Rurutu-Arago, as well as Macdonald and Rarotonga for reference. Moreover, the probability density function of backtracked locations (constructed with a Gaussian kernel) shows four peaks in the distribution that also correspond to the same four present-day hotspots (Extended Data Fig. 5). In addition to the density estimates, a running mean can also be calculated for the backtracked locations and related sample $^{40}Ar/^{39}Ar$ ages. These "age tracks" represent a smoothed estimate of how the hotspot source moved in time, with respect to the applied APM model, which can be thought of a proxy for plume motion in that reference frame.

The results for the various models emphasize the tighter scattering (in blue HIMU-composition around Rurutu-Arago, red-green around Samoa) and shorter plume motion tracks for the new K01m model. This result implies the least amount of plume motion is required for these models, while models that allow for plume motion require a significant amount, but also match predicted plume motion[6,61] back to ~50 Ma for Hawaii and Louisville (Extended Data Fig. 5). Since there are no plate circuits >80 Ma to enable comparison to the Indo-Atlantic hotspot reference frame[38], the modeling results can only be tested against Pacific hotspots.

While testing the model against Rurutu-Arago and Samoa constraints is potentially circular, backtracking the OJP constitutes a more interesting test, as it was previously shown to backtrack 1,200 km away from the closest hotspot at 120 Ma, i.e., Louisville[1]. By defining the outline of the plateau as a series of individual points[76], each individual point is backtracked with the updated K01m APM model. The result shows that the backtracked OJP plateau outline is located directly over the present-day Louisville hotspot (Extended Data Fig. 5). Similarly, the backtracked individual Louisville seamounts are also located over the present-day Louisville hotspot. The updated K01m model thus resolves the north-south discrepancy between modeling predictions of the eruptive location of the OJP and the track of Louisville. The conclusions for a 120 Ma OJP formation also hold for a slightly younger age of formation, recently suggested to be ~116 Ma[52]. In this case, the modeled Louisville hotspot and Eastern Salient of the OJP are still closely spatially associated with each other at ~116 Ma. The revised OJP formation age is similar to that of Seka Seamount, which would further suggest that OJP-Nui formation and initiation of Ellice Basin rifting were simultaneous events. This model represents a fixed hotspot model, while multiple lines of evidence suggest hotspot sources to be mobile[5]. However, motion estimates for Louisville hotspot are within error of its location until at least ~70 Ma[8,9], and older data for greater Ontong-Java Nui are too variable to constrain any possible plume motion. Regardless of a lack of tight paleolatitude constraints, the size of greater Ontong-Java Nui allows for hundreds to thousands of kilometers of plume motion superimposed on our new model, while still maintaining the “end” of the Louisville hotspot track within its outline.

Background Data Sources for Fig. 1

Most of the previously published data used in Fig. 1 were sourced from GEOROC (https://georoc.eu/) precompiled files for ocean islands and seamounts, which were filtered to remove sample data known to be affected by contaminants and/or analytical problems. Non-igneous lithologies were also filtered out. Additional isotope and/or geochronological data were compiled for the Northwest Hawaiian Ridge[77–79], Vlinder Seamount[80], Macdonald Seamount[81], Arago Seamount[82], and Moki Seamount and Rose Atoll[83].

Isotope data groupings used in Fig. 2

The isotopic compositional range spanned by the plateau and smaller structures follow a general temporal pattern. The East Pacific Rise field[84] is given for comparison. The majority of the plateau data from OJP, MP, and HP plots between EM1[57] and a central geochemical component, like FOZO[56]. The OJP data[85–88] consist of the major basement Kwaimbaita and Kroenke components, which represent a relatively high degree of mantle melting with a composition between EM1-FOZO, while the Singgalo component represents a later phase of plateau construction, with a more EM1-rich composition[89] during the LIP stage of the plume. These OJP stages are shown as red fields in Fig. 2, and they are followed by a much later and smaller ~91 Ma alkalic stage[86] (Sigana Formation) that shifted to HIMU[57] compositions (pink field in Fig. 2) in the later stages of OJP activity. Data from MP show basement rock compositional groups similar to the Kwaimbaita/Kroenke and Singgalo lavas at OJP, but recognized[90] as high-Ti EM1-type lavas (dark orange field in Fig. 2), while low-Ti lavas have FOZO-type compositions incorporating potentially a small amount of a HIMU-type source (light orange field in Fig. 2). This HIMU component is also argued to be the primary source for MP late-stage lavas, just as it is at OJP; similarly at HP, the EM1-FOZO main plateau lavas (dark purple, Fig. 2) are followed by the late stage HIMU HP Seamounts[28,86,89,91] (light purple, Fig. 2). Essentially, EM1-FOZO melts were dominant during the voluminous plateau-building stages, while the later, less voluminous stages of volcanic activity shifted to dominantly HIMU-FOZO melts. It is this full range of compositions and transition from plume head (plateau-building) to plume tail (seamount chain-forming) activity that provides the critical context for the potential chemical connection between Louisville Seamounts and OJP-Nui lavas[28], as well as the Ellice Basin seamounts.

Given the well-known challenges involved in linking plateau-forming and seamount-forming phases of mantle plume activity using plate motion models, the Ellice Basin Seamounts and Seka Seamount offer an alternative approach: Their proximity to the OJP and their 90-115 Ma age range provide evidence of a temporal relationship to OJP-Nui (and specifically the OJP), while representing smaller, seamount-forming stages of volcanic activity more directly comparable to the Louisville hotspot track than the plateau-forming melts. The observation that the 90-115 Ma Ellice Basin and Seka seamounts follow the Louisville age progression (Figure 2) and fill in a critical gap along the age progression between Louisville (1 to 79 Ma) and OJP (120 Ma) lends strong support to the hypothesis that these seamounts provide the “missing link” between the Louisville hotspot and OJP.

Ellice Basin Seamounts and Seka Seamount exhibit varying degrees of seawater U enrichment consistent with patterns identified in some Jurassic Pacific MORB[92]. This alteration affects uranogenic ^{206}Pb and to a lesser extent ^{207}Pb, but not thorogenic ^{208}Pb as Th is largely immobile during low-T alteration processes. Thus, seawater U alteration is detectable when samples plot right of the NHRL in $^{208}Pb/^{204}Pb$ versus $^{206}Pb/^{204}Pb$, which over time develops into a broadly horizontal array away from analogous unaltered samples that have retained their primary isotopic composition (Fig. 2). In $^{207}Pb/^{204}Pb$ versus $^{206}Pb/^{204}Pb$, however, affected samples will plot close or slightly under the NHRL, with ingrowth following an isochron consistent with the time of alteration (Fig. 2, top right panel). Samples affected in this manner may, however, remain under-corrected (too radiogenic) as the measured U abundances may not adequately reflect the true ingrowth rate[92]. The Ellice Basin Seamounts scatter right of the FOZO region in $^{208}Pb/^{204}Pb$ versus $^{206}Pb/^{204}Pb$ space, while $^{208}Pb/^{204}Pb$ overlaps with the least radiogenic samples from the Louisville hotspot track[28,93]. Further, in $^{207}Pb/^{204}Pb$ versus $^{206}Pb/^{204}Pb$, the Ellice Basin samples define an array consistent with a 95 Ma isochron from a median Louisville initial Pb composition (Fig. 2) that intersects with age-corrected Louisville hotspot track samples and thus suggests, despite undercorrection for ^{206}Pb ingrowth, the two groups share a genetic link.

The $^{143}Nd/^{144}Nd$ versus $^{87}Sr/^{86}Sr$, the Ellice Basin Seamounts (and Seka) are depleted[14,45], resembling varying mixtures of FOZO and DMM consistent with our conclusions about the original Pb isotope composition of the Ellice Basin and Seka seamounts (Fig. 2). The least radiogenic (age-corrected) Ellice Basin-type samples overlap with the most radiogenic compositions in the Louisville hotspot track field, further corroborating a genetic link between the two groups. The Ellice Basin Seamounts are similar in age to crustal ages inferred for the Ellice Basin itself[68]; thus the Ellice Basin Seamount mantle source melted below young, thin lithosphere. As a result, the Ellice Basin seamount melts likely incorporated a larger proportion of a DMM-type component than the younger Louisville seamounts that erupted below older, thicker lithosphere[93], not unlike increasing proportions of DMM observed in the older stages of the Hawaiian and Louisville hotspot tracks as a function of proximity to a ridge[94,95] (Extended Data Fig. 9). The combination of 1) overlapping componentry between Ellice Basin and Seka seamounts and the Louisville hotspot track, 2) spatiotemporal proximity of the Ellice Basin and Seka seamounts to the OJP, and 3) excellent agreement of Ellice Basin and Seka to our new APM model reconstruction of the Louisville hotspot track (Fig. 1) and age progression (Extended Fata Fig. 8) provide the first robust evidence of the long-proposed link between Louisville and OJP-Nui.

Age corrections to isotope data

Data in Fig. 2 were age corrected to initial isotopic ratios in order to compare isotopic compositions of different temporal groups and/or distinct compositional groups characterized in the OJP, MP, and HP as well as the Louisville hotspot track and Ellice Basin Seamounts. Where possible, ages obtained on specific samples were used to correct their isotopic ratios; for suites with known age constraints, recommended age estimates[28] were used for samples without age determinations. Parent-daughter (P/D) ratios used to calculate the time-integrated ingrowth relative to ^{204}Pb were determined from trace element data and using decay constants of 1.55125×10^{-10} yr^{-1} for ^{238}U, 9.8571×10^{-10} yr^{-1} for ^{235}U, and 4.948×10^{-11} yr^{-1} for ^{232}Th.

All isotope data for the new Wake samples were also age-corrected using the same decay parameters as for the Louisville data, and assumed ages of 100 Ma for the six seamounts to simulate a reasonable estimate of initial ratios. Initial ratios were then forward-modeled to present-day ratios using estimates of parent-daughter ratios of the HIMU mantle source for Pb, Nd, and Hf isotopes[96] and (because Nebel et al.[96] do not provide Rb/Sr ratios) primitive mantle parent-daughter ratios for Sr isotopes[97], following parameters of an identical exercise[14]. These data are reported in Extended Data Table 1.

For most of the new Wake samples, age-corrections to $^{87}Sr/^{86}Sr$, $^{206}Pb/^{204}Pb$, and $^{143}Nd/^{144}Nd$ isotope ratios are large, producing initial isotopic ratios significantly less radiogenic than expected for the modern mantle source. Forward-modeling those initial ratios back to present-day estimates, however, produces model ratios comparable to most of the measured sample data (Extended Data Table 1). Prior modeling on 100 Ma alkali ocean island basalts found similar disagreement between age-corrected and modern isotope ratios, particularly when parent-daughter ratios are high (e.g., Pb isotopes in HIMU melts), yet also good agreement between forward-modeled and measured ratios[98]. This suggests that the utility of age corrections for old alkaline basalts with high P/D ratios may be questionable when the intent is to compare isotopic compositions with their modern counterparts that have undergone little radiogenic ingrowth.

Figure 1 and Extended Data Figure 9 provide examples of the comparability of non-age corrected (i.e., measured) Cretaceous and modern lavas from the Rurutu-Arago hotspot; measured $^{143}Nd/^{144}Nd$ ratios from Cretaceous parts of the hotspot track, for example, closely resemble $^{143}Nd/^{144}Nd$ ratios from the youngest part of the track. Furthermore, trace element data are not available for all previously published isotope data used in this study, and thus age corrections are not possible for all data. For completeness, only measured isotopic ratios are shown in figures discussing seamount geochemistry. The exception is Fig. 2, where a broad range of OJP-Nui-Louisville melts, which represent a range of high and low degree melts and mantle source compositions produced from 120 Ma to present, are shown.

Alteration

Cretaceous seafloor rocks are nearly ubiquitously altered by seawater and various secondary mineralization processes. Abundances of fluid-mobile elements, and correspondingly some parent-daughter ratios of traditional radiogenic isotope systems used to identify mantle sources of intraplate volcanoes, may be modified by these processes. Alternatively, dissolved trace metals in seawater (e.g., Sr, Nd) can overprint the magmatic isotopic signature of a lava. Strong acid leaching is employed to remove secondary isotopic overprints obscuring primary magmatic signatures[29]. However, cryptic alteration of some isotopes and/or time-integrated primary isotopic ratios resulting from modified parent-daughter ratios may also be present, and cannot be restored via leaching.

Trace element ratios such as Th/U and Y/Y* can be used to proxy U mobility and phosphatization processes, respectively. In Extended Data Fig. 10, elevated Th/U correlates with $^{208}Pb/^{204}Pb$ of the Wake samples, but no correlation exists with $^{206}Pb/^{204}Pb$ (but we note that a lack of correlation is not necessarily related to alteration). Regardless, the new Pb isotopic ratios reported here on Wake lavas are consistent with the range defined by younger segments of the Rurutu-Arago hotspot track (Extended Data Fig. 7), so any isotopic modification by seafloor alteration does not cause the new Wake samples to plot outside of the known Rurutu-Arago isotope field. No correlation with Th/U is apparent with $^{143}Nd/^{144}Nd$ or $^{87}Sr/^{86}Sr$. When Y/Y* (a proxy for phosphatization) is plotted (Extended Data Fig. 10), the most radiogenic $^{143}Nd/^{144}Nd$ occurs with the strongest positive Y/Y* anomaly, but no correlation with Pb isotopes is observed. The same pattern is present in the Ellice Basin Group samples (where characterized for bulk compositional data[14]), suggesting that samples with sufficiently high levels of phosphatization develop DMM-like $^{143}Nd/^{144}Nd$, which remains unusually radiogenic even after age correction. Based on trace element evidence, we exclude $^{143}Nd/^{144}Nd$ of phosphatized Ellice Basin and Wake samples from further discussion; data for samples suspected of phosphatization are shown in plots but are distinguished from the other samples. Ellice Basin samples lacking bulk composition data are also flagged in relevant figures because the extent of phosphatization cannot be evaluated for those samples.

Plate motion history and model shown in Fig. 3

The exact plate motions of the pieces of greater Ontong Java Nui are still not well established, however paleomagnetic data of the plateaus, as well as seafloor morphology and ages between the plateaus has led to different suggestions[21,51,67,68]. In the scenario where the OJP was fixed with respect to the Pacific Plate around ~120 Ma, the new model predicts an ~120 Ma eruptive location on the north side. Alternatively, the plateaus rotated around the time of break-up around a rotation axis internal to OJP[51], and the 120 Ma Louisville eruptive location would be approximately central between the three plateaus that separated. Critically, when employing our new absolute plate motion model, the large size of greater Ontong Java Nui contains the original eruptive location of Louisville, regardless of the uncertainties regarding these motions. By ~95 Ma, HP had rifted south, and the Ellice Basin between OJP and MP had mostly opened[67]. The oldest Ellice Basin Seamount (95 Ma) is located on the fossil ridge[14,68] and thus defines a minimum age for final Ellice Basin spreading. An older seamount (Seka, 115 Ma[45]), located near the southern Gilbert Ridge, has a similar isotopic composition to the Ellice Basin Seamounts and is likely genetically related (Fig. 2), a hypothesis supported by the observation that Seka both lies on the new reconstructed hotspot track for Louisville and lies on the Louisville age progression. The presence of this seamount further supports early, rapid opening of the Ellice Basin by the time the main plateau-forming phase of OJP-Nui was waning. By this time, MP had been captured by the Pacific plate[67], so a Louisville track prediction using Pacific plate motion is appropriate. Around ~90 Ma, the exact relationship of the Louisville hotspot to the Osbourn ridge is unclear; volcanoes of this age range have been subducted, and the lack of seafloor magnetic anomalies around the Osbourn Trough makes establishing exact spreading rates within a 95-80 Ma time span difficult. However, motion may still have continued on the Osbourn plate boundary until 79 Ma, after which the entire area was captured by the Pacific plate[67]. At ~79 Ma, the oldest Louisville seamount[8,36] erupted south of the Osbourn Trough, so all of the Louisville seamounts that erupted from that time onward were subjected to Pacific plate motion. Much later, the Tonga trench experienced roll-back, while the Pacific plate continued to subduct, initiating Louisville Seamount subduction around ~5 Ma[99] and continuing today. The "present" panel of Fig. 3 also shows alternative APM model predictions, all reconstructing south of OJP; K01[18]; WK08[39]; T19R: model R[50]; T10corr[100]: subsequently corrected[50]; D12[6].

Data availability

All data generated during this study are included in this published article (and its supplementary information files), and are available in the EARTHCHEM repository (doi will be supplied).

Code availability

The best-fit plate rotation Matlab code is available upon request from the corresponding author.

Author contribution statement

JK and VAF contributed equally to this study. Conceptualization: JK, VAF, MGJ, AAPK. Field expedition and sampling: CK, JK. Sample preparation and data collection: AA, JK, MB. Modeling: JK, PW, AAPK. Writing, editing, and figures (original draft): All authors. Writing, editing, modeling, and figures (revised version): VAF, KK, MGJ, AAPK.

EXTENDED DATA

Extended Data Figures 1-8

Extended Data Tables 1-3

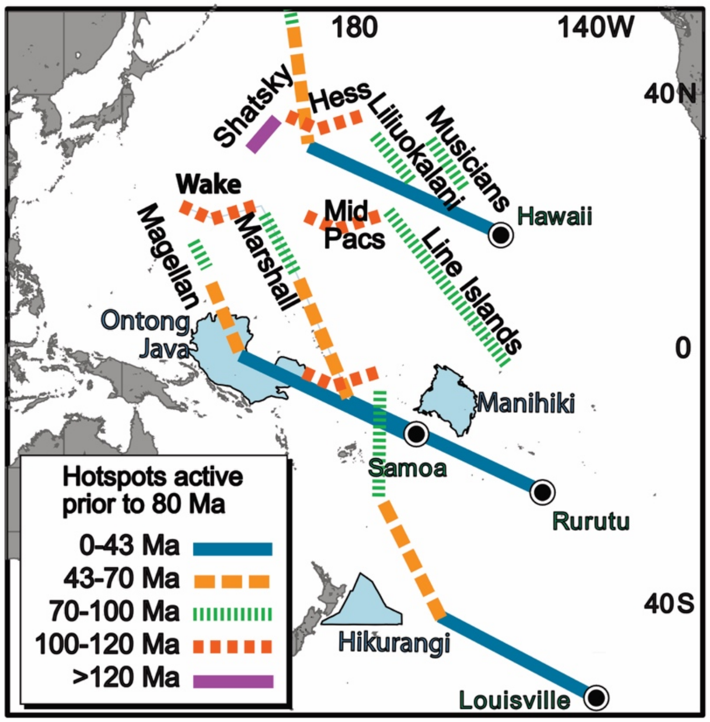

Extended Data Figure 1*. Idealized map of the Pacific Ocean basin, showing relevant hotspot tracks, anchored at present-day locations indicated with black dots. Different sections of the hotspot tracks are color-coded by approximate range in eruption ages*[18]*. In the West Pacific, many sections are represented by seamount groups known by their own names. In light blue, the three oceanic plateaus are shown that are thought to have made up Ontong-Java Nui together.*

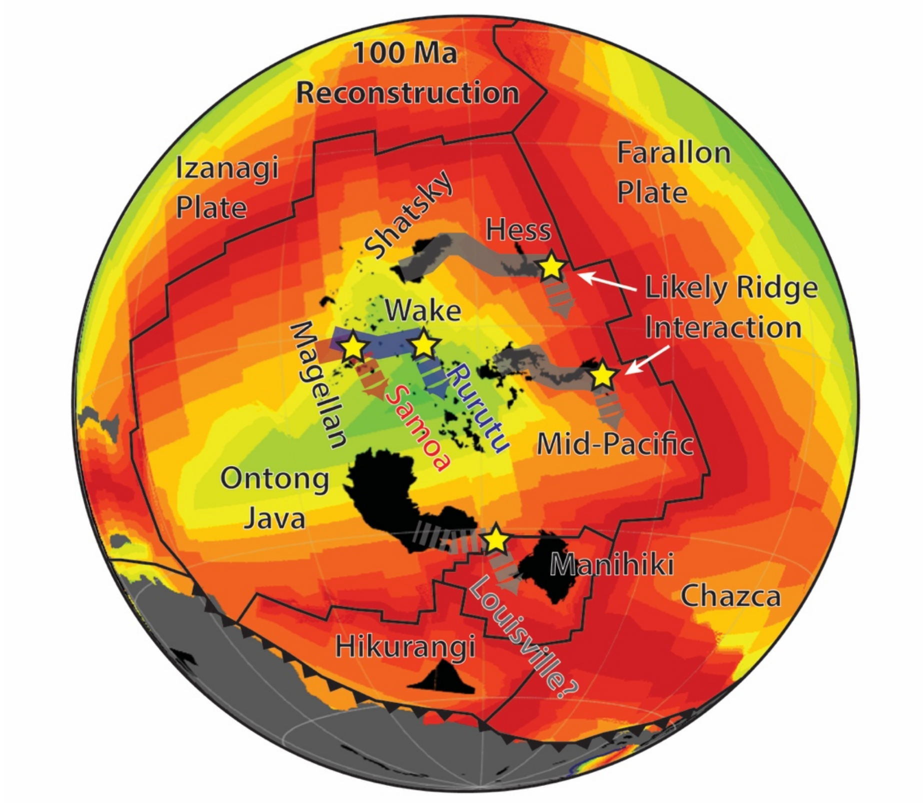

Extended Data Figure 2. *100 Ma plate configuration and relative position of volcanic structures relevant to APM modeling (global projection from GPlates[101]). Shatsky Rise and Mid-Pacific Mountains erupted near a spreading center (likely causing plume motion[5]), while Rurutu-Arago and Samoa erupted within the growing Pacific plate. Louisville's position shows the approximate modeled track for the updated model rotation.*

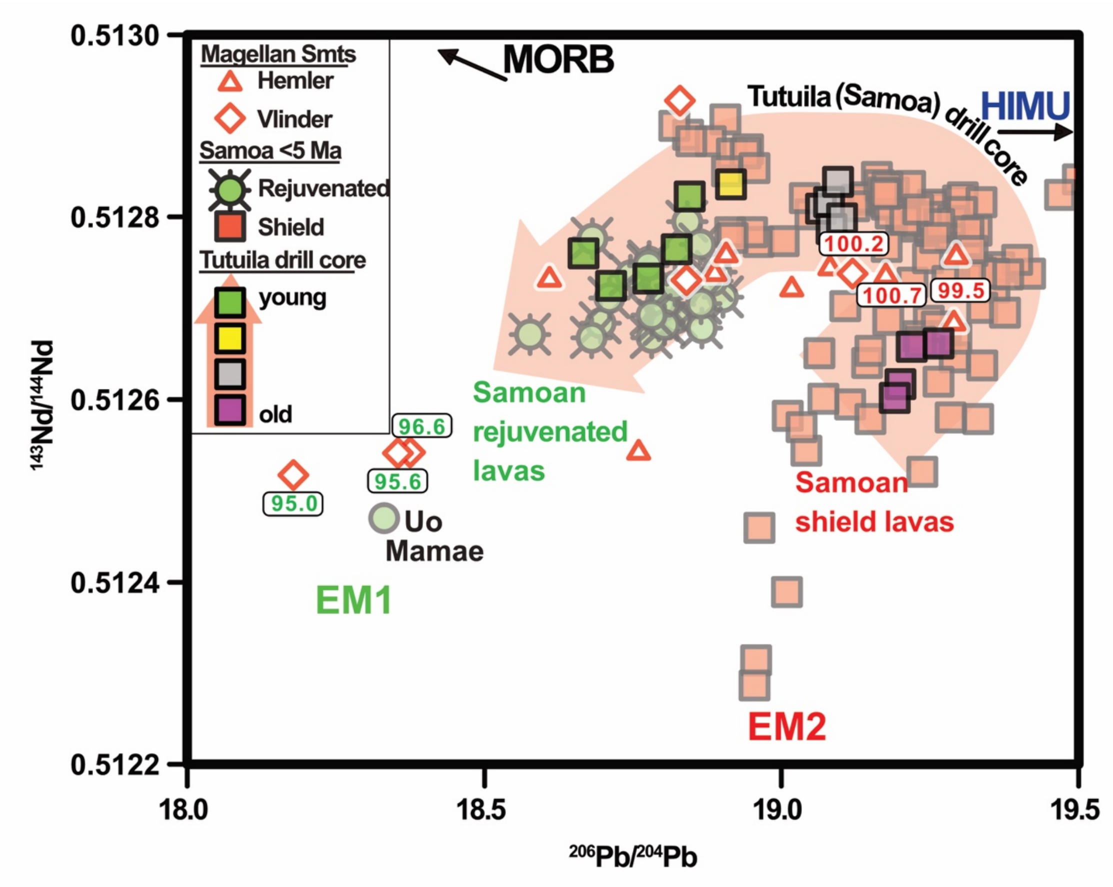

Extended Data Figure 3. *Compositional overlap between modern Samoa (< 5 Ma) and Cretaceous Samoan volcanoes—Hemler and Vlinder seamounts—in the West Pacific. Most of the geochemical evolution of Samoan volcanoes through time is reflected in a drill core into Tutuila Island (Samoa[47]). This shows (red arrow) a change in lava compositions from shield to rejuvenated lavas, with volcanoes active over the past 5 Ma[72]. The older samples[29,59] (ages shown in white text bubbles) from Hemler and Vlinder (~100 Ma) mainly plot around the shield lavas in Samoa while the youngest samples (~95 Ma) continue through the rejuvenated lavas represented by the most extreme EM-1 type composition in the Samoan area (Uo Mamae[102]).*

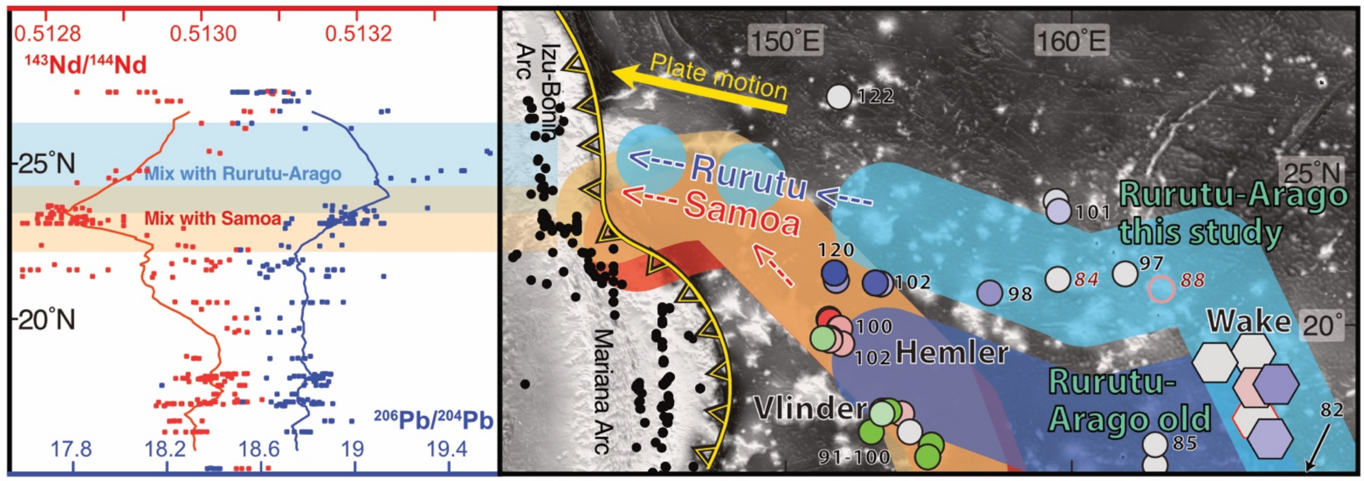

Extended Data Figure 4. *Map of West Pacific seamounts, showing Rurutu-Arago and Samoa predicted hotspot tracks (K01[18] in dark shade, this study in light shade). Black numbers with white outline represent ages[29,73], while numbers in red represent likely unrelated volcanic ages, given large age difference with expected age along the hotspot track and difference in composition (pink circle[29]). New Pb isotope data (hexagons) provides the "missing link" that suggests that Rurutu hotspot continues through the seamounts west of Wake Island. The samples outlined with red has $^{143}Nd/^{144}Nd$ affected by phosphatization. The existing (dark blue[18]) APM model track for the Rurutu-Arago hotspot is devoid of major seamounts, while the new track (light blue) continues the unusual isotopic composition and morphological chain to the Izu-Bonin-Mariana trench. A similar prediction for Samoa (red: K01[18]; orange: updated) shows both hotspots have a corresponding unusual spike in isotopic compositions in the arc (left panel; lines represent running means), indicating prior subduction of a continuing chain of similar composition, mixing Rurutu-Arago (HIMU) or Samoa (EM2) hotspot material into the mantle wedge.*

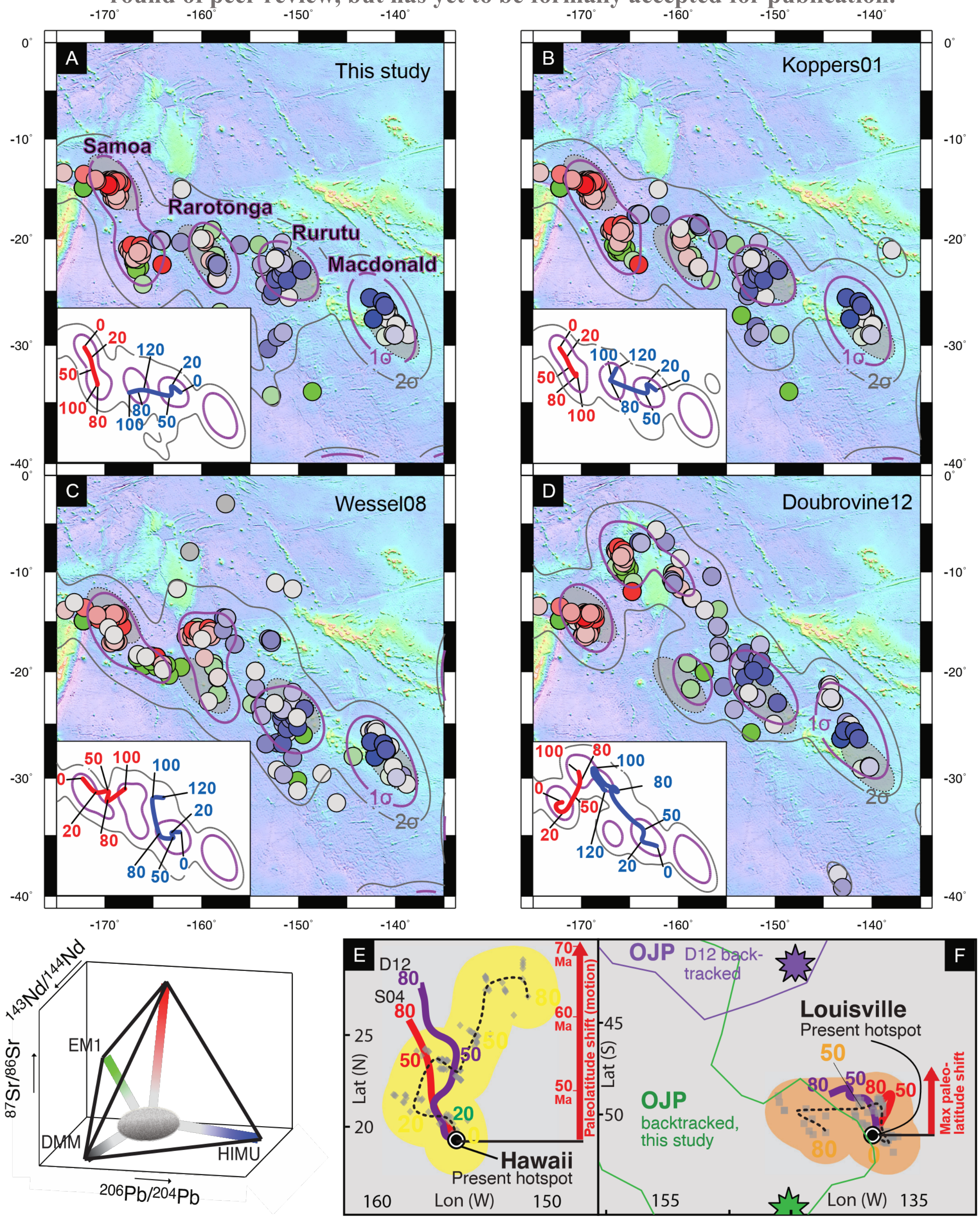

Extended Data Figure 5. *Backtracked original eruptive locations for Samoa and Cook-Austral-related volcanoes (Cook-Austral, Samoa, Tuvalu, Gilbert, Wake, Magellan, Tokelau), using various absolute plate motion models (a. this study; b. Koppers01[18]; c. Wessel08; d. Doubrovine12[6]). Backtracked seamounts color-coded (lower left panel) for their isotopic compositions show that at present-day* *hotspots (purple text) are the focus of clusters of consistent geochemical compositions, defined by grey (2) and purple (1) contours for Gaussian-kernel probability density estimates for the backtracked locations. Insets show these density contours and the running mean of backtracked location and age to estimate plume motion from model mismatch from fixed hotspots (a-d). Backtracked (grey symbols[6]) locations for Hawaii (e) and Louisville (f) and their smoothed age-track (wide yellow or orange) highlight a deviation from predicted plume motion (S04/red[61] and D12/purple[6]) beyond 50 Ma, indicating a mismatch for plate motion models into the Cretaceous. Outlines show Ontong-Java Plateau (OJP) backtracked with the new model overlap with Louisville, where stars show approximate center of Ontong-Manihiki-Hikurangi. Red arrows show smoothed tracks match derived latitudinal plume motion from paleomagnetic latitudes[13,103] . Backtracking of OJP assumes fixed relationship to the Pacific plate, with no rotation of the plateau[1].*

This is a preprint of an article that has been submitted to Nature, and revised based on one round of peer review, but has yet to be formally accepted for publication.

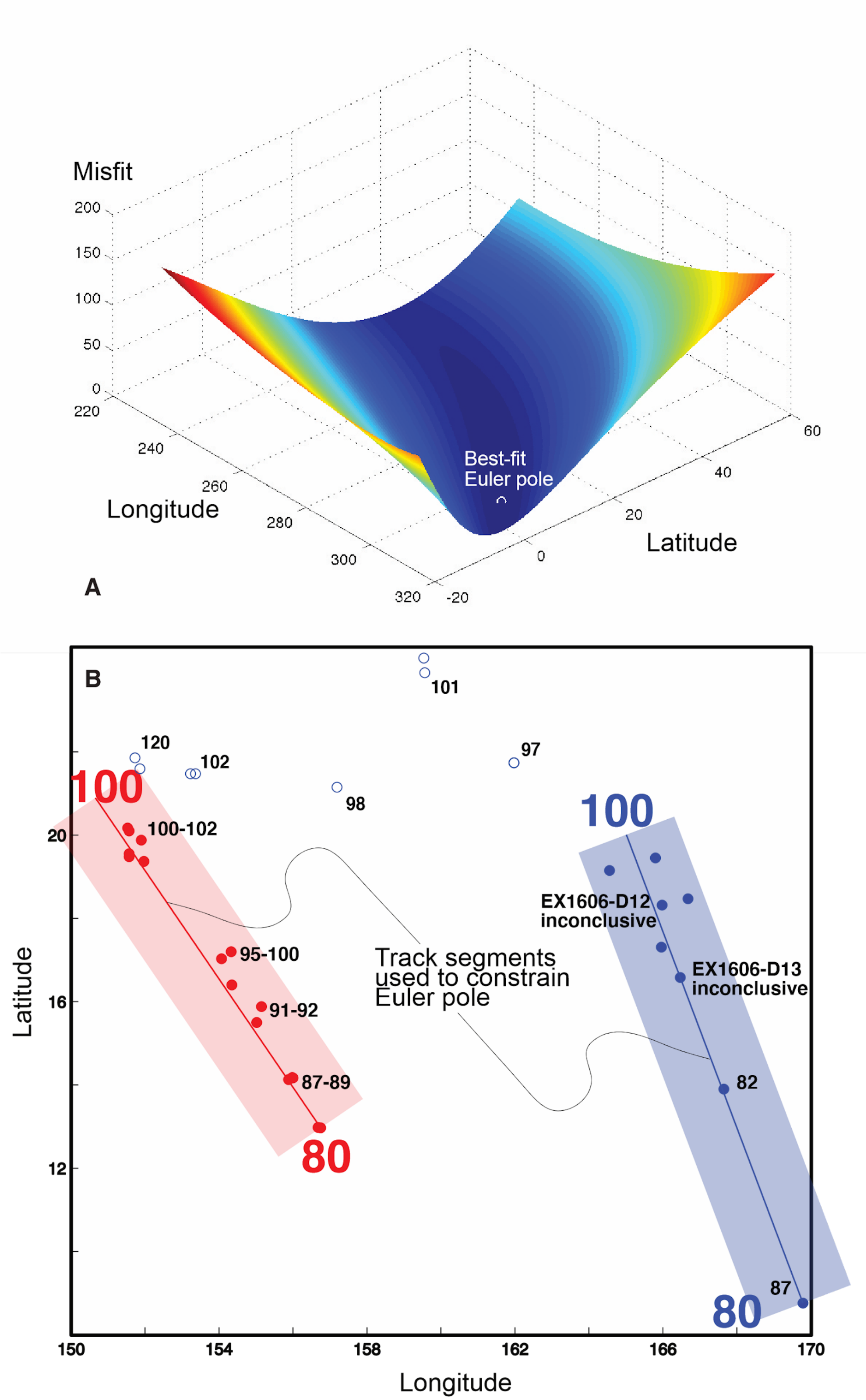

Extended Data Figure 6*. Rotation (Euler) pole modeling is accomplished by a grid search for the best-fit pole (5°N, 306°E), shown as the latitude-longitude location for which the minimum misfit is found (white dot). Constraints for the modeled rotation are the colored seamount locations (blue and red, selected based on their apparent fit in composition), and the approximate age range for these volcanic tracks (80 -100 Ma), based on model-specific and adjacent seamount volcanic ages*[29,59] *(black numbers next to seamount markers). Only two samples from EX1606 had material suitable for age dating, but results lacked a statistically robust plateau and were therefore inconclusive. Open circles represent Wake area seamounts and their ages, predating the 80 – 100 Ma time period modeled.*

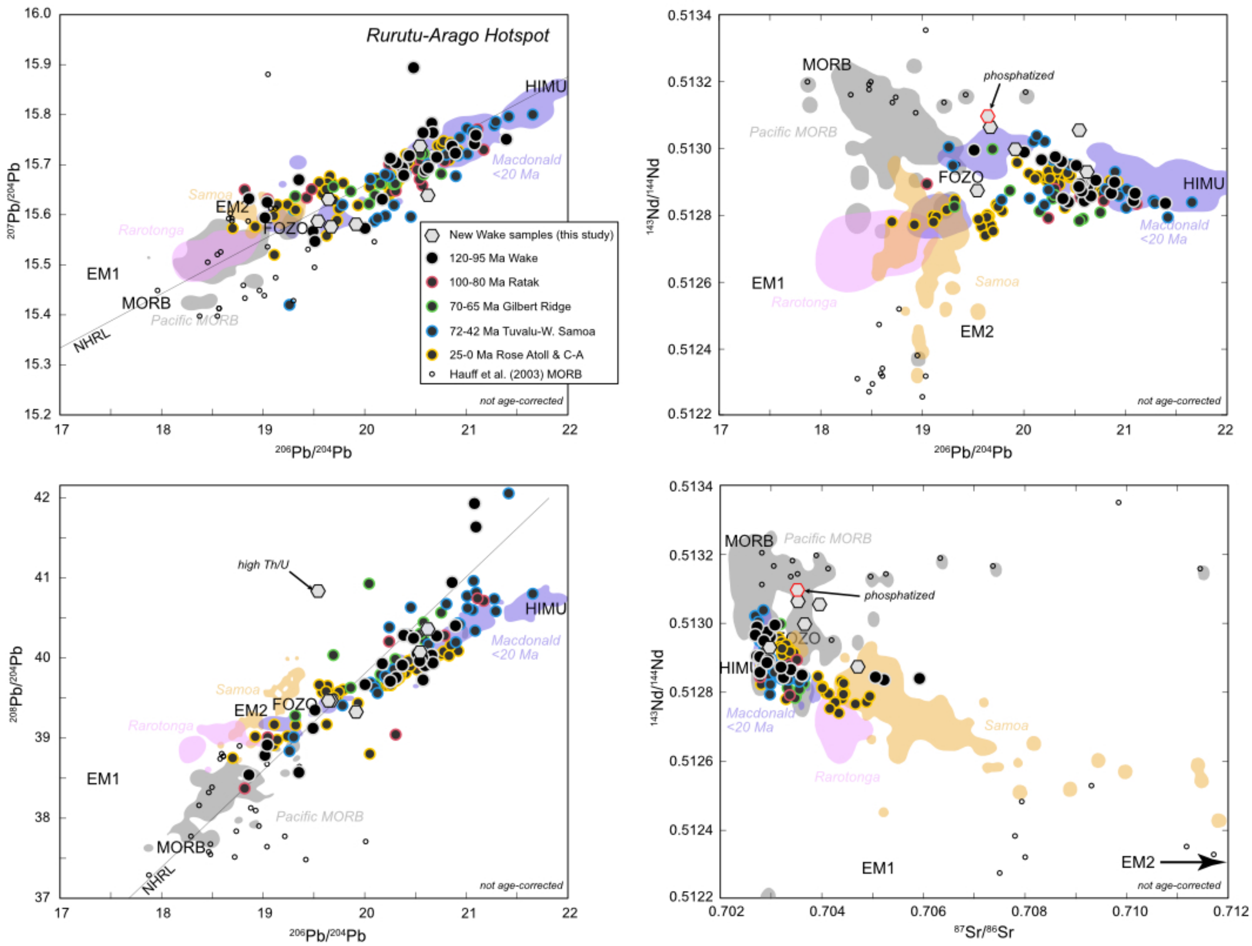

Extended Data Figure 7. *Non-age-corrected plots of* ***A)*** *$^{207}Pb/^{204}Pb$ vs. $^{206}Pb/^{204}Pb$,* ***B)*** *$^{208}Pb/^{204}Pb$ vs. $^{206}Pb/^{204}Pb$,* ***C)*** *$^{143}Nd/^{144}Nd$ vs. $^{206}Pb/^{204}Pb$, and* ***D)*** *$^{143}Nd/^{144}Nd$ vs. $^{87}Sr/^{86}Sr$ of our new Wake seamount samples (hexagons) compared to published data for the Tuvalu, Gilbert Ridge, Marshall/Ratak, and Wake Seamount portions of the Rurutu-Arago track (circles). Background data for young segments of the Cook-Austral plumes (Macdonald, Rurutu-Arago, Rarotonga), the Samoan plume, and Pacific MORB are given as 2SD contours of KDEs of their respective datasets. Jurassic Pacific MORB data with seawater U alteration[92] is also shown as small black open circles. A 2SD contour of the KDE for published Wake seamounts is shown as an open grey contour. In both plots, the new Wake data plots within the known compositional range for the Wake Seamounts and the greater extent of the track. One of the new samples has unusually high $^{208}Pb/^{204}Pb$; this is a signature occasionally expressed in older Rurutu-Arago lavas and persists after strong leaching[14]. Here, $^{208}Pb/^{204}Pb$ is positively correlated with*

Th/U (see Extended Data Table 1), indicating U loss during alteration. Data are not corrected for post-eruptive radiogenic ingrowth (see Methods).

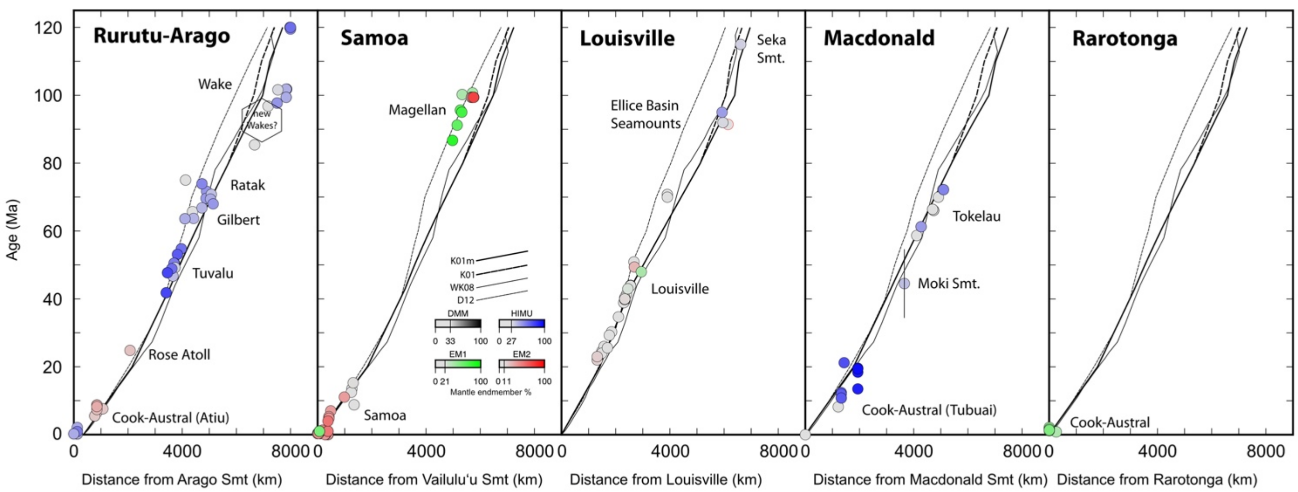

Extended data Figure 8. *Age-distance relationships of the Rurutu-Arago, Samoan, Louisville, Macdonald, and Rarotonga plumes (see Background Data Sources For Figures in Methods). Data shown here are only samples with age determinations or published age estimates (where well constrained by nearby volcanoes[14,28] and Sr-Pb-Nd data to permit color coding. APM models are also included for reference (WK08[39] = Wessel and Kroenke, 2008; D12[6] = Doubrovine et al., 2012 without plume drift correction; K01[18] = Koppers et al., 2001; K01m = modified Koppers et al., 2001 from this study). The oldest portions of the Hotspot Highway are in good agreement with K01m model predictions; some scatter occurs as a function of plume drift (e.g., Cretaceous portion of the Samoa hotspot; see Extended Data Figure 5). For four of the five hotspots shown here, the data are consistent with age progressions that can be traced back into the Cretaceous. Rurutu-Arago and Macdonald have HIMU to FOZO-like compositions, while Samoan volcanoes are EM-type to FOZO in composition. While the Macdonald track appears to have not existed prior to 72 Ma, the Rurutu-Arago age progression can be clearly traced into the Wakes and back to ~120 Ma. The Samoan plume was active during the Cretaceous, forming the Magellan chain in the West Pacific where EM2 and EM1 compositions consistent with those found in Samoan shield and rejuvenated volcanoes, respectively (see Extended Data Figure 3 for details). The FOZO Louisville hotspot track and older Ellice Basin*

Seamounts as well as Seka Seamount; which are likely FOZO-to-DMMlike with Pb isotopes partly overprinted by seawater U ingrowth, are also age-progressive. The Rarotonga plume is only known from two young volcanoes in the Cook-Australs.

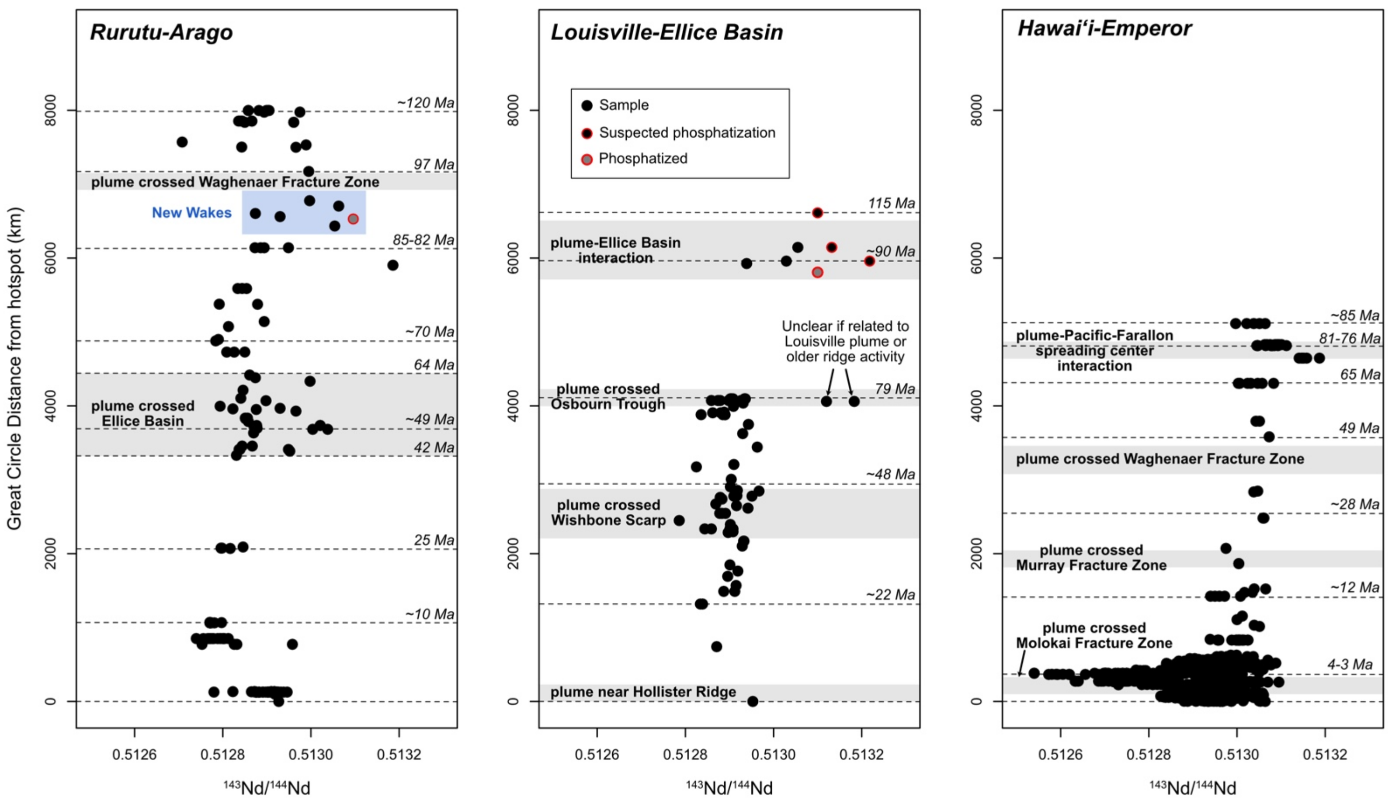

Extended Data Figure 9. *Great circle distance (km) from active hotspot center vs. $^{143}Nd/^{144}Nd$ (not age-corrected) for the (left) Rurutu-Arago, (center) Louisville-Ellice Basin Seamounts, and (right) Hawaii-Emperor hotspot tracks. Isochrons are provided as dashed lines, and light grey fields mark where the plumes interacted with ridges or fracture zones. All three hotspot tracks record significant variability in isotopic composition over time that correspond to interaction of the plume with major lithospheric structural features. Rurutu-Arago, which was a true-intraplate hotspot for the entirety of its documented history, produced episodes of depleted (high $^{143}Nd/^{144}Nd$) melts that coincide spatially with major lithospheric structures, but otherwise maintains a fairly constant $^{143}Nd/^{144}Nd$ over time. Samples with evidence of phosphatization (high Y/Y* and/or P_2O_5; see Extended Data Figure 10) are shown as light grey circles with red outlines. Black circles with red outlines are samples that may have been phosphatized ($^{143}Nd/^{144}Nd > \sim 0.5131$) but cannot be confirmed due to lack of available major and trace element data. By contrast, the Louisville hotspot track, including the Ellice Basin Seamounts,* *records a long-term trend of enrichment with time that records its transition from plume-ridge interaction to true intraplate. Deviations also occur when the plume crossed the Osbourn Trough (however, it remains unclear whether this is related to the Louisville plume), and later the Wishbone Scarp (attributed to source mantle heterogeneity; Beier et al., 2011; Vanderkluysen et al., 2014). The broad enrichment trend in Louisville is similar to long-term enrichment observed in the Hawaiian plume, which also interacted with a ridge in the Cretaceous before transitioning to a true-intraplate plume system (Regelous et al., 2003). Data sources are the same as in Fig. 1."*

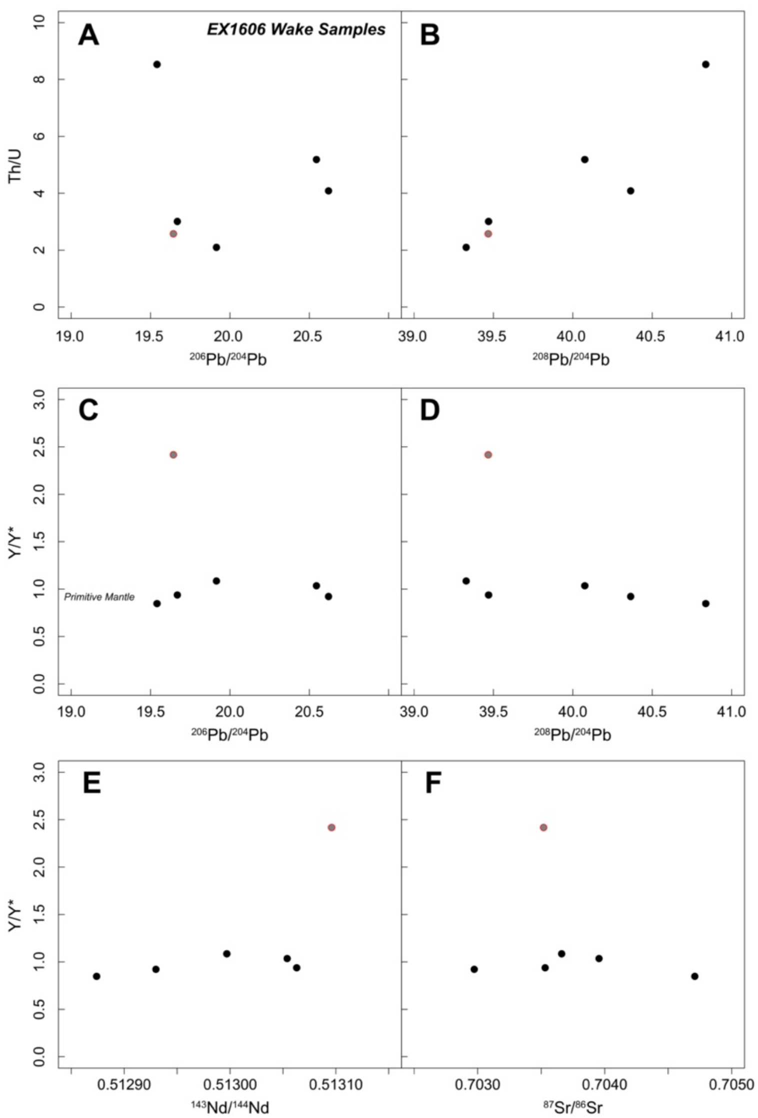

Extended Data Figure 10. *Trace element alteration proxies versus Sr-Nd-Pb isotope compositions of the new Wakes (EX1606) samples.* ***A)*** *Th/U versus measured $^{206}Pb/^{204}Pb$,* ***B)*** *Th/U versus measured $^{208}Pb/^{204}Pb$, and* ***C-F)*** *Y/Y* versus radiogenic isotope compositions. Versus Th/U, $^{206}Pb/^{204}Pb$ (**A**) exhibits only a weak correlation with Th/U, while $^{208}Pb/^{204}Pb$ (**B**) is much more strongly correlated,* *indicating modification of U abundances in the EX1606 samples.* $^{143}Nd/^{144}Nd$ ***(E)*** *exhibits some correlation versus Y/Y*, a proxy for phosphatization, becoming more radiogenic at high Y/Y**, while Pb and Sr isotopes show no correlation.*

Extended Data Table 1. Geochemical compositions for Wake area seamounts

	units	D5-3	RSD	D6-4	RSD	D7-1	RSD	D10-1	RSD	D12-1	RSD	D13-1	RSD
Seamount name		McDonnell Guyot		unnamed W		Lafayette Smt		unnamed S		unnamed SW		Batfish Smt	
Latitude		19.15152		19.44748		17.30973		18.46733		18.31973		16.58102	
Longitude		164.55802		165.79677		165.96018		166.67875		165.97903		166.47195	
Majors Elements (LIBS)													
SiO_2		53.3		54		47.2		53.8		47		58.5	
TiO_2		3.0		2.1		3.3		2.8		3.3		1.7	
Al_2O_3		16.8		16.9		17.1		16.7		15.5		18.8	
Fe_2O_3		8.4		8.8		11.7		8.9		12.4		4.5	
MgO		3.5		3.8		4.7		3.6		6.2		2	
CaO		9.6		8.2		12.8		8.4		11.9		8.3	
Na_2O		3.5		4.2		2.5		3.7		2.7		4	
K_2O		1.9		2.1		0.6		2.2		1.1		2.1	
Total		100		100.1		99.9		100.1		100.1		99.9	
Trace Elements (LA-ICP-MS)													
	units		**RSD**		**RSD**		**RSD**		**RSD**		**RSD**		**RSD**
Y	ppm (ug/g)	20.84	1.5	12.95	1.3	118.3	3.4	34.23	1.6	29.69	1.8	24.52	1.4
Zr	ppm (ug/g)	176.3	1.9	127.9	1.5	195.9	2.7	513.7	0.9	276.4	1.6	209.4	1.2
Yb	ppm (ug/g)	1.455	1.4	0.881	3.0	4.456	3.7	2.529	1.0	1.728	2.3	2.374	2.0
W	ppm (ug/g)	0.436	4.0	0.417	2.9	0.795	3.6	0.555	2.5	0.698	3.2	0.418	1.4
Rb	ppm (ug/g)	54.09	2.4	44.97	1.2	49.33	2.8	29.32	2.3	14.97	1.7	62.52	1.1
Sr	ppm (ug/g)	300.6	2.1	295.6	2.0	413.5	3.3	1134	1.5	182.3	1.4	310.0	1.0
Nb	ppm (ug/g)	33.06	1.4	19.21	2.2	40.52	3.2	150.3	1.0	77.61	1.3	72.21	1.2
Mo	ppm (ug/g)	0.911	2.5	1.611	2.0	2.029	3.6	2.521	1.9	2.791	0.9	0.463	1.1
Mo	ppm (ug/g)	0.951	1.5	1.625	3.4	2.031	3.0	2.558	1.4	2.854	1.3	0.473	1.9
Cd	ppm (ug/g)	0.118	4.5	0.117	9.1	0.140	2.9	0.280	3.3	0.236	4.6	0.097	4.4
Sn	ppm (ug/g)	1.656	2.2	1.127	3.3	1.677	3.5	2.546	2.4	2.323	1.3	1.900	0.8
Sb	ppm (ug/g)	3.512	1.5	2.940	2.2	7.086	3.4	1.434	1.0	2.646	1.2	0.583	2.0
Cs	ppm (ug/g)	2.364	1.8	1.287	2.0	2.012	4.5	0.634	0.6	0.404	2.2	0.533	1.0
Ba	ppm (ug/g)	125.8	1.7	129.3	3.1	248.5	3.7	574.7	0.9	198.7	2.2	675.0	1.3
La	ppm (ug/g)	16.71	1.7	11.34	2.3	90.09	3.2	84.21	1.0	39.78	1.9	27.51	1.7
Ce	ppm (ug/g)	31.35	1.6	24.89	1.8	43.30	2.2	168.6	1.1	87.34	2.1	50.58	1.5

Pr	ppm (ug/g)	4.348	2.3	3.135	1.7	10.64	3.1	18.16	1.2	11.37	1.7	5.732	2.0
Nd	ppm (ug/g)	18.10	1.8	13.25	1.8	42.58	4.4	66.45	1.5	48.76	3.1	21.24	2.2
Sm	ppm (ug/g)	3.948	1.5	3.022	2.3	7.121	3.8	11.24	1.2	10.74	1.6	4.167	1.6
Eu	ppm (ug/g)	1.429	1.5	1.171	2.3	2.363	3.7	3.546	1.8	3.181	1.8	1.933	1.7
Gd	ppm (ug/g)	4.070	1.6	3.084	1.2	9.366	3.8	10.62	1.6	10.23	2.0	4.352	1.6
Tb	ppm (ug/g)	0.590	2.0	0.442	2.5	1.233	4.2	1.331	1.3	1.336	1.8	0.650	2.2
Dy	ppm (ug/g)	3.316	2.3	2.441	1.7	7.653	4.6	6.641	1.1	6.560	1.5	3.951	1.7
Ho	ppm (ug/g)	0.649	1.7	0.456	2.0	1.829	3.9	1.212	0.8	1.092	1.5	0.829	1.4
Er	ppm (ug/g)	1.722	1.7	1.132	2.6	5.372	4.1	3.081	1.2	2.494	1.9	2.403	1.5
Tm	ppm (ug/g)	0.237	2.0	0.149	2.0	0.728	4.2	0.414	1.4	0.300	2.0	0.362	1.7
Lu	ppm (ug/g)	0.212	1.9	0.119	1.1	0.728	4.0	0.351	1.9	0.228	1.6	0.364	1.1
Hf	ppm (ug/g)	4.221	2.1	3.111	1.8	4.652	4.9	9.905	0.9	6.337	1.7	4.449	1.6
Ta	ppm (ug/g)	2.068	2.3	1.124	1.5	2.346	3.2	8.855	1.5	4.404	1.6	4.013	0.6
Pb	ppm (ug/g)	1.623	1.9	1.043	2.1	4.602	4.0	6.936	1.3	3.604	2.1	2.440	1.5
Bi	ppm (ug/g)	0.020	1.9	0.012	11	0.020	4.8	0.048	2.9	0.025	5.1	0.019	2.2
Th	ppm (ug/g)	1.787	1.3	1.122	1.6	2.067	4.1	11.07	1.2	5.851	1.9	3.578	1.5
U	ppm (ug/g)	0.852	1.4	0.373	1.9	0.803	5.1	2.711	1.7	0.686	2.1	0.690	1.4
MgO	wt %	1.835	1.6	1.241	1.6	1.287	0.9	2.965	2.4	6.997	1.5	0.504	3.3
Al_2O_3	wt %	13.15	1.7	14.05	1.1	12.74	1.8	17.60	2.5	11.59	1.7	18.36	3.0
CaO	wt %	3.920	1.6	4.939	1.8	6.371	1.3	5.124	2.3	11.02	1.6	4.456	3.5
Sc	ppm (ug/g)	18.18	1.4	21.09	2.0	18.38	1.4	7.480	1.1	23.54	1.4	4.682	3.1
TiO_2	wt %	3.112	1.3	2.105	2.5	2.658	1.3	2.968	1.6	3.212	1.4	1.417	3.2
V	ppm (ug/g)	124.7	2.3	117.9	1.8	200.5	0.9	140.7	1.7	277.9	1.9	18.16	3.4
Cr	ppm (ug/g)	41.44	3.1	308.4	1.7	386.6	0.8	7.815	4.1	696.1	2.2	1.194	10.3
MnO	wt %	0.066	1.4	0.138	1.1	0.092	0.8	0.094	0.9	0.118	2.3	0.068	3.1
Fe_2O_3	wt %	9.893	2.1	11.18	1.8	11.42	1.8	8.456	1.3	13.57	2.7	4.479	2.4
Co	ppm (ug/g)	22.28	1.5	56.30	1.6	28.56	2.0	21.62	1.2	35.65	2.3	5.295	3.2
Ni	ppm (ug/g)	41.08	1.2	86.20	2.0	60.54	1.7	22.76	2.5	177.9	1.8	4.571	4.8
Cu	ppm (ug/g)	114.3	1.2	82.69	1.2	168.6	0.9	30.54	2.1	64.58	2.0	14.07	4.6
Zn	ppm (ug/g)	191.2	1.6	158.1	2.0	175.9	2.0	288.0	2.1	189.2	1.2	90.73	3.8
Th/U		2.10		3.00		2.57		4.09		8.53		5.19	
Y/Y*		1.09		0.94		2.42		0.92		0.85		1.04	
Isotope Data (MC-ICP-MS)			**2SE**		**2SE**		**2SE**		**2SE**		**2SE**		**2SE**
$^{206}Pb/^{204}Pb$		19.915	4E-04	19.669	5E-04	19.644	6E-04	20.621	3E-04	19.541	1E-03	20.545	4E-04
$^{207}Pb/^{204}Pb$		15.581	3E-04	15.576	5E-04	15.631	6E-04	15.639	3E-04	15.587	1E-03	15.737	4E-04
$^{208}Pb/^{204}Pb$		39.328	9E-04	39.469	1E-03	39.467	2E-03	40.364	9E-04	40.837	2E-03	40.075	1E-03
$^{143}Nd/^{144}Nd$		0.512997	7E-06	0.513063	7E-06	0.513096	4E-06	0.512930	3E-06	0.512874	5E-06	0.513054	6E-06

$^{87}Sr/^{86}Sr$	0.703661	7E-06	0.703531	6E-06	0.703519	7E-06	0.702973	6E-06	0.704709	7E-06	0.703955	7E-06
$^{176}Hf/^{177}Hf$	0.282956	3E-06	0.283030	5E-06	0.282948	3E-06	0.282974	3E-06	0.282929	3E-06	0.282931	3E-06
Initial Ratios (100 Ma)												
$^{206}Pb/^{204}Pb_i$	19.333		19.272		19.451		20.188		19.330		20.232	
$^{207}Pb/^{204}Pb_i$	15.553		15.557		15.622		15.618		15.577		15.722	
$^{208}Pb/^{204}Pb_i$	38.938		39.088		39.308		39.798		40.262		39.556	
$^{143}Nd/^{144}Nd_i$	0.51291		0.51297		0.51303		0.51286		0.51278		0.51297	
$^{87}Sr/^{86}Sr_i$	0.70294		0.70292		0.70304		0.70287		0.70438		0.70315	
$^{176}Hf/^{177}Hf_i$	0.28294		0.28302		0.28291		0.28296		0.28292		0.28291	
Calculated P/D Ratios												
$^{238}U/^{204}Pb$	37.221		25.399		12.376		27.713		13.488		20.041	
$^{235}U/^{204}Pb$	0.270		0.184		0.090		0.201		0.098		0.145	
$^{232}Th/^{204}Pb$	78.632		76.837		32.077		114.039		115.953		104.740	
$^{147}Sm/^{144}Nd$	0.1373		0.1437		0.1053		0.1065		0.1387		0.1236	
$^{87}Rb/^{86}Sr$	0.51		0.43		0.34		0.07		0.23		0.57	
$^{176}Lu/^{177}Hf$	0.00700		0.00535		0.02181		0.00494		0.00501		0.01139	
Forward-modeled Ratios												
$^{206}Pb/^{204}Pb_f$	19.780		19.719		19.898		20.635		19.777		20.679	
$^{207}Pb/^{204}Pb_f$	15.575		15.579		15.644		15.641		15.599		15.744	
$^{208}Pb/^{204}Pb_f$	39.516		39.666		39.886		40.377		40.840		40.134	
$^{143}Nd/^{144}Nd_f$	0.51305		0.51311		0.51317		0.51300		0.51293		0.51312	
$^{87}Sr/^{86}Sr_f$	0.70306		0.70304		0.70316		0.70299		0.70450		0.70327	
$^{176}Hf/^{177}Hf_f$	0.28300		0.28308		0.28297		0.28302		0.28298		0.28297	

Major elements collected by laser induced breakdown spectroscopy, using a Nd-YAG 20 mJ pulsed laser and a Catalina Scientific EMU-120 echelle spectrometer. Major element compositions were calibrated against 36 different standards, using partial least squares (PLS) regression, in Matlab. Predicted compositions of unknown samples using PLS show typically <2 wt.% variability on repeat analyses, after each sample is re-normalized to 100% total values. Trace element data were obtained using a ThermoFinnegan Element2 ICP-MS (University of South Carolina). The sample powders were dissolved in Teflon-distilled HF:HNO_3 mixture, subsequently dissolved in 2 wt.% HNO_3, and spiked with In at 2 ppb concertation in the solution. The USGS reference material BHVO-2 was used as a standard and the reference materials BCR-2 and JB-2 were run as unknowns along the samples. The calculated concentrations for the unknowns agree well within 5% for most elements relative to the recommended concentrations from GEOREM (accessed, August 2022[104]). Pb isotope compositions were acquired with a Nu Plasma HR MC-ICP-MS (University of Hawai‘i at Mānoa), using sample standard bracketing, and Tl doping to monitor fractionation. Pb was separated and purified with Sr resin and AG1 resin[53]. Repeatability of Pb isotope analysis of a given sample is typically about +/- 1e-3. Compositions are normalized to values[105] for NIST 981 Pb. The Sr and Nd fractions were further processed at the University of South Carolina. Sr samples were purified with Sr-Spec resin in HNO_3. For Nd, the REE fractions were separated from major element matrix via TRU-spec resin in HNO_3 and HCl media, and Nd separated from the other REE on an LN-resin using 0.25N HCl. Hf was isolated from the matrix on LN resin from the fractions recovered from the washes of the TRU spec column[106]. Sr, Nd and Hf isotope ratios were were acquired using a ThermoFinnegan Neptune multicollector. Repeated analyses of SRM987 dispersed with the samples gave $^{87}Sr/^{86}Sr = 0.710321 \pm 0.000007$, (2 stdev, n=11). The data are reported relative to the recommended SRM987 $^{87}Sr/^{86}Sr_{SRM987} = 0.71025$. Nd isotopes were corrected for fractionation using $^{146}Nd/^{144}Nd = 0.7219$ and repeated analyses of the JNdi-1 reference material yielded an average $^{143}Nd/^{144}Nd = 0.512102$ +/- 0.000005 (2σ, n=11). The Nd data are reported relative to the accepted value for JNdi-1 of $^{143}Nd/^{144}Nd = 0.512115$. Hf isotopes were corrected for fractionation using $^{179}Hf/^{177}Hf = 0.7325$. An in-house Hf standard solution was determined at $^{176}Hf/^{177}Hf = 0.282142 \pm 0.000006$ (2σ, n=8), which corresponds to the original JMC 475 solution value of $^{176}Hf/^{177}Hf = 0.282163$. The data is reported relative to the accepted JMC 475 value of $^{176}Hf/^{177}Hf$ 0.282160[107]. BCR-2 duplicates are duplicate analyses of the same digestion.

Extended Data Table 2. Stage poles for the Modified Pacific Hotspot Reference Frame Absolute Plate Motion Model (italics from K01[18])

Stage start (Ma)	Stage end (Ma)	Latitude (°N)	Longitude (°E)	Rotation Rate (°/Myr)	Standard Deviation
0	*20*	*70.1*	*302.0*	*0.88*	*0.016*
20	*43*	*67.1*	*294.5*	*0.58*	*Not given*
43	*80*	*18.8*	*253.6*	*0.66*	*0.029*
80	100	5.0	306.0	0.85	0.13
100	*110*	*75.1*	*44.8*	*0.44*	*Not given*
110	*125*	*65.3*	*273.2*	*0.45*	*0.042*

Extended Data Table 3. Locations used to constrain the revised 100-80 Ma stage pole.

	Latitude (°N)	Longitude (°E)
Magellan Seamounts:		
1	20.17	151.53
2	19.48	151.57
3	19.55	151.57
4	20.1	151.57
5	19.88	151.9
6	19.37	151.97
7	17.03	154.07
8	17.2	154.33
9	16.4	154.35
10	15.5	155.02
11	15.88	155.15
12	14.13	155.88
13	14.18	155.98
14	14.17	156
15	12.98	156.68
16	12.97	156.75
Marshall Seamounts:		
17	19.15	164.56
18	19.45	165.8
19	17.31	165.96
20	18.32	165.98
21	16.58	166.47
22	18.47	166.68
23	13.9	167.65
24	8.76	169.79

Extended Data Table 4. Standard data.

	Quality Control			duplicate	duplicate	**Quality Control**		
	BCR-2	**n=2**		BCR-2	BCR-2	**JB-2**	**n=2**	
Trace Elements (LA-ICP-MS)								
	[Lit]	[Calculated]	%Recovery			[Lit]	[Calculated]	%Recovery
Y	36.07	36.57	101%			23.56	25.12	107%
Zr	186.5	190.1	102%			48.25	46.69	97%
Yb	3.392	3.269	96%			2.529	2.481	98%
W	0.465	0.507	109%			0.308	0.309	100%
Rb	46.02	50.22	109%			6.4	7.065	110%
Sr	337.4	349.5	104%			175.2	192.5	110%
Nb	12.44	12.36	99%			0.565	0.477	84%
Mo	250.6	251.9	101%			1.014	0.960	95%
Mo	250.6	253.3	101%			1.014	0.981	97%
Cd	0.69	0.620	90%			0.3	0.114	38%
Sn	2.28	2.153	94%			0.635	0.615	97%
Sb	0.302	0.256	85%			0.261	0.209	80%
Cs	1.16	1.134	98%			0.8	0.868	108%
Ba	683.9	683.6	100%			218.1	218.7	100%
La	25.08	25.04	100%			2.281	2.254	99%
Ce	53.12	53.04	100%			6.552	6.354	97%
Pr	6.827	6.854	100%			1.129	1.138	101%
Nd	28.26	28.00	99%			6.392	6.074	95%
Sm	6.547	6.379	97%			2.266	2.177	96%
Eu	1.989	1.998	100%			0.836	0.825	99%
Gd	6.811	6.781	100%			3.123	2.886	92%
Tb	1.077	1.044	97%			0.586	0.554	95%
Dy	6.424	6.328	99%			3.868	3.923	101%
Ho	1.313	1.287	98%			0.863	0.860	100%
Er	3.67	3.560	97%			2.537	2.517	99%
Tm	0.534	0.513	96%			0.393	0.376	96%
Lu	0.505	0.481	95%			0.389	0.372	96%
Hf	4.972	4.788	96%			1.487	1.396	94%
Ta	0.785	0.755	96%			0.040	0.037	94%
Pb	10.59	10.49	99%			5.25	5.01	95%
Bi	0.05	0.06	116%			0.031	0.03	99%
Th	5.828	5.76	99%			0.258	0.25	96%
U	1.683	1.56	93%			0.153	0.14	89%
MgO	3.599	3.82	106%			4.43	5.58	126%
Al_2O_3	13.48	13.98	104%			14.62	16.30	111%
CaO	7.114	7.59	107%			9.852	10.74	109%
Sc	33.53	35.52	106%			54.08	62.56	116%
TiO_2	2.265	2.34	103%			1.167	1.17	100%
V	417.6	436.3	104%			572.4	607.9	106%
Cr	15.85	15.54	98%			26.65	24.85	93%
MnO	0.200	0.21	103%			0.213	0.23	109%
Fe_2O_3	13.77	14.24	103%			14.28	14.91	104%
Co	37.33	39.30	105%			37.57	38.20	102%
Ni	12.57	12.07	96%			14.77	13.52	92%
Cu	19.66	18.08	92%			222.1	236.2	106%
Zn	129.5	149.76	116%			110.4	122.2	111%

Isotope Data (MC-ICP-MS)						
$^{206}Pb/^{204}Pb$	18.758	3E-04				
$^{207}Pb/^{204}Pb$	15.618	3E-04				
$^{208}Pb/^{204}Pb$	38.725	7E-04				
$^{143}Nd/^{144}Nd$	0.512643	6E-06	0.512646	6 E-06	0.512643	5E-06
$^{87}Sr/^{86}Sr$	0.705014	6E-06	0.705005	7E-06	0.705010	9E-06
$^{176}Hf/^{177}Hf$	0.282868	5-06	0.282869	7E-06	0.282870	4E-06